Journal of Geochemical Exploration 185 (2018) 14–32

Contents lists available at ScienceDirect

Journal of Geochemical Exploration

journal homepage: www.elsevier.com/locate/gexplo

Compositional fingerprints of chromian spinel from the refractory chrome ores of Metalleion, Othris (Greece): Implications for metallogeny and deformation of chromitites within a "hot" oceanic fault zone

Argyrios Kapsiotis[a,*], Anne Ewing Rassios[b], Ibrahim Uysal[c], Giovanni Grieco[d], Recep Melih Akmaz[e], Samet Saka[c], Micol Bussolesi[d]

[a] School of Earth Science and Geological Engineering, Sun Yat-sen University, 510 275 Guangzhou, PR China
[b] Institute of Geology and Mineral Exploration, Lefkovrisi, 50100 Kozani, Greece
[c] Department of Geological Engineering, Karadeniz Technical University, TR-61080 Trabzon, Turkey
[d] Department of Earth Sciences, University of Milan, via S. Botticelli, 23-20133 Milan, Italy
[e] Department of Geological Engineering, Bülent Ecevit University, 67100 Zonguldak, Turkey

ARTICLE INFO

Keywords:
Laser-ablation ICP-MS
Chromian spinel (Cr-spinel)
Chromitite
Ophiolite
Othris
Greece

ABSTRACT

The chrome ores of the retired Metalleion mine of the Othris ophiolite are hosted in a small volume of a pervasively serpentinized, tabular harzburgite body. These ores have been studied to determine their geological mode of occurrence, mineralogy and chromian spinel (Cr-spinel) chemistry. The ores consist of massive chromitite (85–95% modal Cr-spinel) with mylonitic fabric in imbricate-shaped pods. Chromian spinel displays a limited range in Cr# [Cr/(Cr + Al) × 100 = 53–63] and Mg# [Mg/(Mg + Fe^{2+}) × 100 = 59–73] and low TiO_2 content (≤ 0.11 wt%). Minor- (Ti, Ni, V, Mn and Zn) and trace-element (Sc, Co and Ga) concentrations do not show any significant variations from Cr-spinel cores to boundaries and were not considerably modified by post-magmatic processes. However, Cr-spinel compositions show slight enrichments in Zn and V, and depletions in Ti and Sc when compared to the composition of chromite from the East Pacific Rise mid-ocean ridge (MOR) basalts. The composition of Cr-spinel from the Metalleion chromitites is quite anomalous on a global perspective as these ores are not clearly associated to a suprasubduction zone (SSZ) or MOR chemistry.

Field data indicate that the Metalleion chromitites lack remnant dunite envelopes due to prolonged shearing within the deforming harzburgite host and are constrained in location to a ductile-brittle shear zone that correlates with the transforming direction of the Domokos oceanic fault. Compositional data indicate that chromitites equilibrated with ambient harzburgite via a melt-peridotite interaction process followed by melt mixing. Geochemical calculations demonstrate that the parental magmas of the Metalleion chromitites had intermediate affinity between typical mid-ocean ridge basalts (MORB), island arc tholeiites (IAT) and boninites. We conclude that these melts originated within a hydrated and oxidized mantle wedge beneath an infant forearc basin connected by a transform fault to an active MOR.

1. Introduction

Ore bodies made up of variable proportions of Cr-rich spinel are dubbed in the literature as chromitites (e.g., Stowe, 1994). A special category of chromitites includes those chrome ores that occur near the boundary between the oceanic crust and the lithospheric mantle (e.g., Rollinson, 2008), and less frequently in the lower parts of the crustal sequence of ophiolites (e.g., Arai et al., 2004). These chromitites are commonly referred to as ophiolitic or podiform, though the latter term does not always appear to be morphology-dependent.

The rudimentary mineralogical constituent of ophiolitic chromitites is chromian spinel (Cr-spinel; henceforth this designation denotes a mineral with wide but variable composition in the central domain of the $MgAl_2O_4$-$FeAl_2O_4$-$MgCr_2O_4$-$FeCr_2O_4$ plane). Chromian spinel is the main reservoir of Cr in nature and a highly refractory igneous mineral that is customarily regarded as an important petro- and metallogenetic indicator (e.g., Dick and Bullen, 1984; Kamenetsky et al., 2001; Rollinson, 2008). The major-element composition of Cr-spinel has been vastly employed to decipher the geochemical affinity of the melts in equilibrium with chromitites at the time of their precipitation (e.g.,

* Corresponding author at: Independent researcher, Ayiou Mina 31, Salamis 18900, Greece.
E-mail address: kapsiotis@mail.sysu.edu.cn (A. Kapsiotis).

https://doi.org/10.1016/j.gexplo.2017.11.003
Received 3 September 2017; Accepted 5 November 2017
Available online 08 November 2017
0375-6742/

Maurel and Maurel, 1982; Zaccarini et al., 2011). The inferred parental magmas of chromitites commonly have arc-related signatures (González-Jiménez et al., 2014); necessitating that a suprasubduction zone (SSZ) setting may be a critical aspect of the genesis of ophiolitic chromitites (e.g., Zhou et al., 1996).

Laser ablation-inductively coupled plasma-mass spectrometry (LA-ICP-MS) has become the method of choice for the in situ analysis of minor and trace elements in Cr-spinel from ophiolitic chromitites (e.g., Pagé and Barnes, 2009). This method allows the measurement of variations in the absolute concentrations of a suite of minor and trace elements (i.e., Ni, V, Zn, Sc, Co, Ga etc.) in Cr-spinel that can aid us decipher the petrological mechanisms that govern the formation of chromitites (e.g., Zhou et al., 2014). Minor and trace elements in Cr-spinel are sensitive to even slight fluctuations of physicochemical parameters related to mantle melting (T, P and fO_2; e.g., Dare et al., 2009). For that reason, these elements are invaluable in documenting the metallogeny of ophiolitic chromitites and determining the composition and origin of their parental melts (e.g., González-Jiménez et al., 2014).

Though Cr-spinel is customarily regarded as a resistant mineral, it is has been recognized that various post-magmatic processes (i.e., subsolidus re-equilibration, metamorphism) can modify its original igneous signatures (e.g., Barnes, 2000; Barnes and Roeder, 2001). Such processes result in conversion of Cr-spinel to porous ferrous chromite and/or ferrian chromite (e.g., Gervilla et al., 2012) commonly along grain boundaries and brittle fractures leaving the inner parts of Cr-spinel grains practically unaffected (e.g., Mukherjee et al., 2010). However, Cr-spinel with unusually high contents of minor elements (Mn, Ni, Co, Zn and Ti) in the core has been reported from several metamorphosed chromitites [i.e., Tidding Suture Zone, eastern Himalaya (Singh and Singh, 2013); eastern Rhodope Metamorphic Core complex, southern Bulgaria (Colás et al., 2014)]. From this perspective, in situ LA-ICP-MS analysis can serve as a safer method for the identification of post-magmatic processes that modify Cr-spinel composition and cannot be easily revealed using electron probe micro-analysis (EPMA).

Herein, we examine the origin of the chromitite bodies from the Metalleion mine in the Domokos area, West Othris ophiolite, Greece. The study of the Metalleion chromitites will aid significantly in the resolution of the puzzling petrogenetic evolution of the Othris mantle as these ores are not compositionally associated with a SSZ chemistry nor do they ″fit″ any existing lithospheric stratigraphic or structural ophiolitic model. The principal goals of this renewed investigation are: i) to explain the geological process(es) that could have aided the ″mechanical″ concentration of chromitites within the Metalleion peridotite body; ii) to provide unpublished mineral-chemical (EMPA, LA-ICP-MS) data that could help us further the metallogenetic understanding of these chromitites; and iii) to compare our results with those from the study of chromitites from other localities on a global basis in order to generate a more complete image of Cr mineralization within a characteristic mid-ocean ridge (MOR) -type lithospheric sequence represented by the West Othris.

2. Geological investigation

2.1. Geological outline of the Othris ophiolite complex

Ophiolites of continental Greece occur as two NNW-SSE trending belts, namely the Jurassic Western Hellenic Ophiolite (WHO) belt and the Jurassic-Early Cretaceous Eastern Hellenic Ophiolite (EHO) belt placed to the west and east side of the Pelagonian boundary, respectively (Fig. 1). The WHO represent remnant slices of the Pindos-Neotethyan oceanic lithosphere once developed between the continental margins of Pelagonia and Apulia (e.g., Moores, 1969; Smith and Rassios, 2003). Among the WHO the Othris ophiolite (Fig. 1), in central Greece, represents a mid-Jurassic lithospheric slab emplaced to the east onto the passive margin of the Pelagonian platform (Smith et al., 1975). This lithospheric section crops out over an area of > 900 km^2 and is dominated by (fertile) mantle lithologies. In structural terms it consists of a series of thrust sheets overlain by Cretaceous conglomerates and limestones, flysch and Oligocene-Miocene molasse-type sedimentary formations (Hynes, 1972; Smith et al., 1975; Fig. 2).

The Othris ophiolitic sequence is itself imbricated so that each nappe has been emplaced in reverse stratigraphic order (Rassios and Konstantopoulou, 1993). From the top of the ophiolitic pile to its base, the nappes consist of the following lithospheric sections: (1) a sheet dominated by refertilized peridotites (i.e., Mega Isoma ultramafic body) overlying a (2) spinel-bearing harzburgite nappe (i.e., Metalleion ultramafic body) that overthrusts (3) near-Moho peridotites, (4) ultramafic and gabbroic cumulates, (5) sheeted dikes and (6) pillow lavas and flows occasionally including ridgecrest-derived hydrothermal Cu deposits (Smith, 1979; Smith and Rassios, 2003). These nappes are emplaced over older lava and chert formations [the Agrilia formation of Smith, 1979] most likely associated with Permo-Triassic rifting and oceanic sedimentation along the west margin of the Pelagonian continental mass (Menzies and Allen, 1974; Fig. 2). Below these nappes a chaotic lithological mixture of ophiolitic rocks with pelagic sediments apparently represents a leftover of an accretionary mélange generated in a convergent plate margins setting during obduction (i.e., Agoriani mélange; Ferrière et al., 1988). Amphibolite outcrops near Lamia and Metalleion have been interpreted as remnants of a sub-ophiolitic metamorphic sole. Dating of amphiboles from these rocks using the $^{40}Ar/^{39}Ar$ isotopic pair method yielded obduction instigation ages at 169 ± 4 Ma (Spray et al., 1984). Nowadays the entire nappe association is found tectonically emplaced to the SW over the Eocene flysch (Rassios and Konstantopoulou, 1993; Fig. 2).

The genesis of the Othris ophiolite and the evolution of its nappe system are difficult to explain. The west part of the ophiolite complex has been mostly described as a typical section of MOR-type lithosphere (e.g., Barth et al., 2003). In contrast, the ophiolitic rocks of the eastern domains of Othris show MOR and SSZ geochemical affinities (e.g., Barth et al., 2008). The precise mechanism that induced the dual geochemical character to the East Othris ophiolites, but left those of West Othris practically unaffected from any SSZ-related magmatic event, remains hotly debated until present.

2.2. Historical overview of the Othris chrome ore mines – field work

Chrome ore deposits within Othris are much rarer in comparison to Vourinos (NW Greece). This has been attributed to predominance of fertile peridotites in the mantle section of Othris (Menzies, 1973). Despite this pessimistic metallogenetic association ten localities with significant chrome ore occurrences are known from Othris with three of them (Ayios Stefanos, Eretria and Metalleion) hosting economically viable chrome ore bodies (Fig. 2). Approximately 1.5 Mt. of refractory grade (/Al-rich) chrome ore were exploited from the Othris chromitites between 1891 and 1995. Nowadays the Ayios Stefanos ores are almost entirely exhausted. Detailed mapping and drilling exploration in Eretria and Metalleion confirm combined reserves in excess of 0.75 Mt. with geological predictions adding > 1 Mt. to potential raw ore estimates (Rassios et al., 2003).

The Metalleion mine is located in the central part of Othris [latitude (φ): 39° 4.786′ N, longitude (λ): 22° 19.190′ E; Fig. 2], approximately 500 m to the east of the homonymous village covering an area of ~0.2 km^2 (Fig. 3a). In Metalleion mining was done via underground tunneling and by an open pit (350 × 400 m) intersecting some of the old excavation tunnels. Until the early 90′s all the exposed chromitites in the open pit have been excavated leaving minor spoil tips and empty quarry sites. Mining activities stopped in 1991 when the mine was officially shut down. The quarry pit is at present covered by a lake (Fig. 3a) making access to the underwater tunnels practically unfeasible.

The Metalleion mine is placed in the south of the Domokos

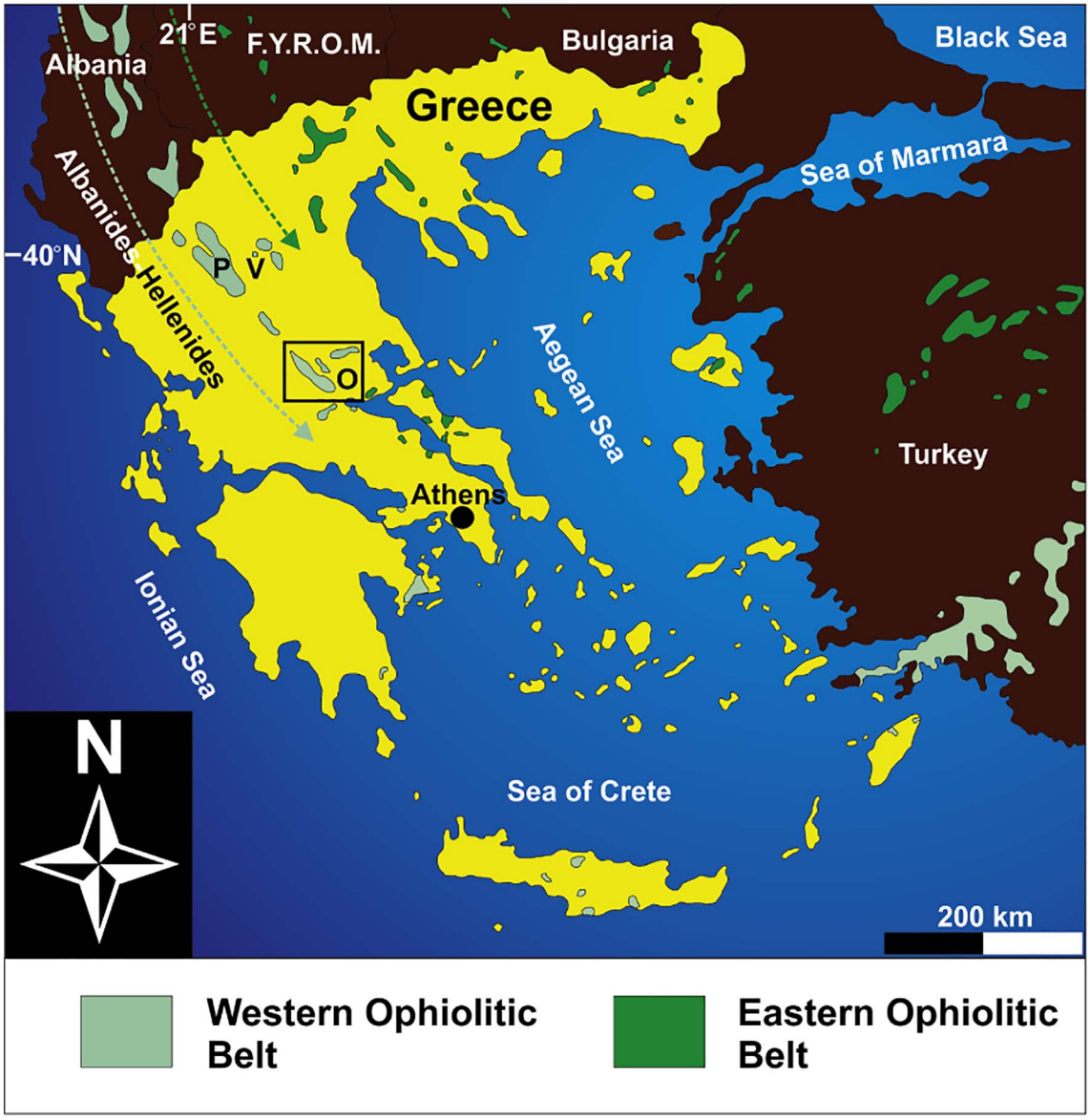

Fig. 1. Outline map showing the distribution of ophiolites in the southern part of the Balkan Peninsula (Vergely, 1976). Both Western Hellenic Ophiolites (WHO) and Eastern Hellenic Ophiolites (EHO) are shown with different colors. Key to lettering for Mesohellenic ophiolites: *V* Vourinos, *P* Pindos, *O* Othris.

ultramafic massif (Fig. 3b). A pervasively sheared harzburgite body (450 thick), with a high-*T* blocky orthopyroxene fabric similar to that of the Vourinos harzburgites, comprises the dominant lithology of the Domokos peridotite nappe (Fig. 3b). Small shows of chromite occurrences crop out at three localities within the Domokos harzburgite nappe. Rich-in-magnetite gabbros and pyroxenites intrude a ductile deformed zone along the western margin of the Domokos massif. Toward the east side of the harzburgite body (not mappable) carbonates and shale sediments of the Othris group occur as the footwall to the nappe, whereas toward the west an imbricate of dolerite lavas and dykes are overlain the ultramafic nappe. Transgressive Cenomanian limestones have been deposited onto the NW side of the Domokos peridotite nappe. Lower topographic regions in the hills of the Domokos plateau are covered by Quaternary deposits including clays, sands and gravels.

The host lithologies of the Metalleion mine area include a series of pervasively brittle- sheared and imbricated serpentinized harzburgites. Historic descriptions indicate that the distribution of ores within harzburgites was largely controlled by deformation. Most of the chromitite bodies were clustered along a (roughly 0.8 km long) tectonically constrained discontinuous ore zone (Fig. 4a) trending almost WSW-ENE and plunging 25°-60° NE along apparent internal thrust surfaces (Fig. 4b). Some of the ore bodies within this zone demonstrate *z*-fold morphologies (Fig. 4b) suggesting displacement toward the NE.

Old photos and geological reports reveal that the chrome ores at Metalleion consisted of elongated ("sausage"-type) pods of massive chromitite ranging in diameter from a few tens of cm to a few m (Fig. 5a). Today only a few small (< 2 m across) chromitite boulders remain within the quarry talus (Fig. 5b) precluding the direct recognition of any genuine geological relation between the peridotite host and the chrome ores. Only in a few chromitite boulders part of the "host" lithology has been preserved. Mesoscopic (and petrographic) observations in these boulders confirm that the ores were in immediate contact with an intensely sheared and pervasively serpentinized-rodingitized harzburgite matrix (Fig. 5b).

Within a few remaining mine talus boulders subrounded to egg-shaped blocks of harzburgite and chromitite (of cm- to tens of cm-scale) can be recognized within a pulverized and strongly altered peridotite matrix (Fig. 5c). These blocks are haloed by cm-scale black-colored reaction rims made up of serpentine ± chlorite (Fig. 5d). The peridotite

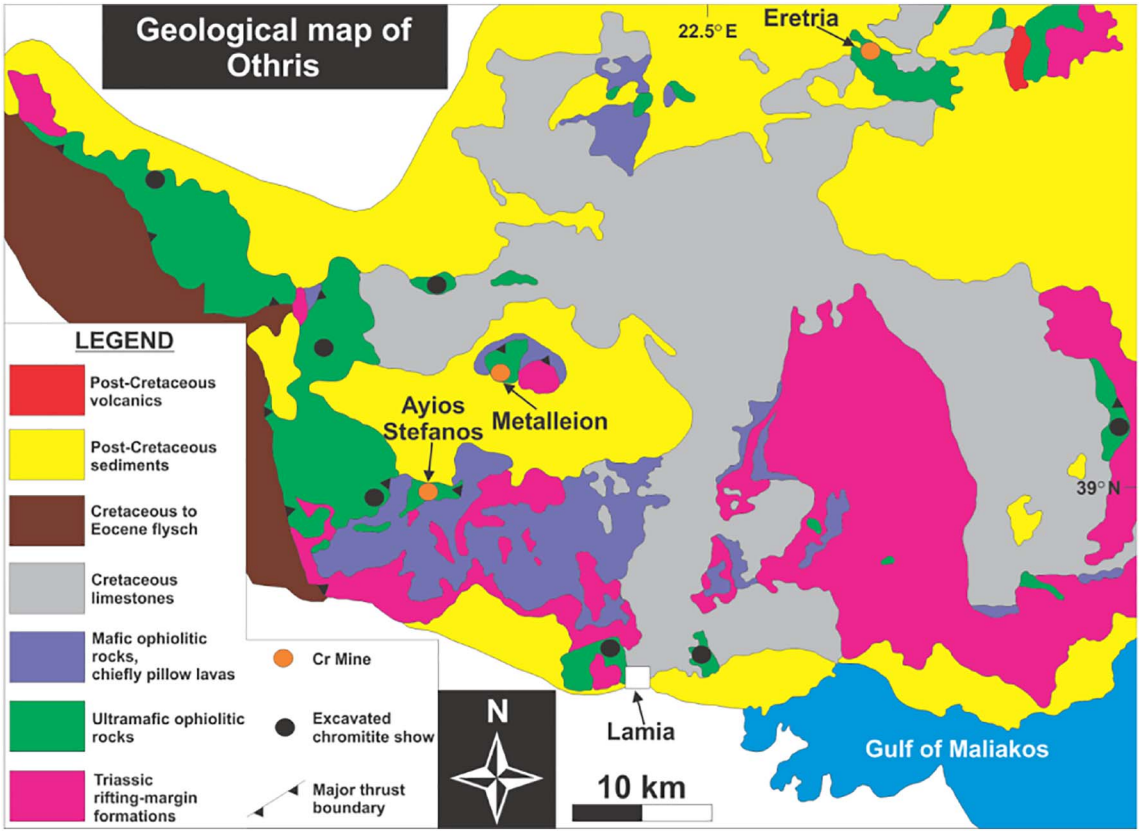

Fig. 2. Geological map of the Othris ophiolite complex (Rassios and Konstantopoulou, 1993).

matrix is pervasively intruded by thin (≤ 0.5 mm) rodingite veinlets (Fig. 5d). Some of the rodingite microveins intrude the serpentinized matrix and the harzburgite pods cutting the reaction rims. None of the veinlets themselves appear to be deformed but intrude into pre-existing brittle fractures.

Occasionally mafic (basaltic) dykes (≤ 10 cm) intrude the serpentinized harzburgite outcrops in the north side of the study area. Some of these dykes have been affected by ductile deformation similar to that of the host peridotite, whereas some others are undeformed. Late brittle fractures (1–5 cm thick) are imprinted on both chromitites and host serpentinites and are filled by calcite most likely precipitated from groundwater originating in limestone.

3. Chrome ore sampling – laboratory methods

Though some specimens and mineral analyses remain from earlier exploration studies additional sampling was undertaken to determine the variation of Cr-spinel chemistry within the chromitite quarry. A total of 12 massive chromitite samples were collected from 6 ore boulders in the quarry talus (2 samples from each boulder).

One polished thin section was prepared for each chromitite sample and was studied under both reflected and transmitted light using an OLYMPUS BX51 optical microscope. The micro-textural characteristics of the specimens were investigated employing a CARL ZEISS SIGMA scanning electron microscope (SEM) at the School of Earth Science and Geological Engineering, Sun Yat-sen University (SYSU), Guangzhou, China. Element-distribution maps of altered Cr-spinels were done using the energy-dispersive spectroscopy (EDS) analytical mode of the same apparatus. To avoid effects of varying experimental conditions each Cr-spinel grain was scanned for the same time and single-element profile line scans were done with constant signal amplification.

Quantitative analyses of major and minor elements in Cr-spinel and ferrian chromite from 6 chromitite samples (each one taken from a different boulder) were performed using a CAMECA SX-100 electron-probe micro-analyzer (EPMA), operating in the wavelength-dispersive spectroscopy (WDS) analytical mode, at the Department of Earth and Environmental Sciences, Ludwig Maximilian University, Munich, Germany. Conditions for spinel analyses were 15 kV excitation voltage and 20 nA beam current with a beam diameter of 1 μm. The peak and background counting times were 10 and 5 s, respectively. Spinels was analyzed using the *Kα* line for Mg, Si, Ca, Al, Ti, V, Cr, Mn, Fe, Ni and Zn. Calibrations were carried out using the following (natural and synthetic) reference materials: andradite for Ca, Si and Fe; corundum for Al; periclase for Mg; rutile for Ti; chromite for Cr; NiO for Ni; sphalerite for Zn; pyrophanite for Mn and vanadinite for V. The detection limits are listed in the following as percentages by mg/Kg [or parts per million (ppm, 10^{-6} Kg)]: Mg = ca. 350, Al = ca. 350, Si = ca. 270, Fe = ca. 800, Ca = ca. 200, Ti = ca. 280, V = ca. 380, Cr = ca. 1100, Zn = ca. 1400, Mn = ca. 1000 and Ni = ca. 1250. Both Fe^{3+} and Fe^{2+} in Cr-spinel and ferrian chromite were calculated assuming ideal spinel stoichiometry (XY_2O_4). These (are approximate detection limits that) were automatically calculated taking into account the following parameters: (1) the intensity of the characteristic X-ray of the analyzed element, (2) the average X-ray intensity and (3) the counting time of the background signal, and (4) the element concentration in the standard material. Data were corrected following the PAP (Pouchou and Pichoir, 1985) correction procedure. Micro-analyses of silicate minerals and accessory Cr-spinel in harzburgite were done using a CAMECA SX-100 electron-probe micro-analyzer (EPMA) at the University of Edinburgh (UK) using the analytical conditions presented above. Micro-analyses of major- and minor-element oxides in Cr-spinel and ferrian chromite in chromitites as well as representative micro-analyses of silicates and accessory Cr-spinel in the harzburgite host are given as different Microsoft Office Excel spreadsheets in a single supplementary file.

Concentrations of minor and trace metals in Cr-spinel were

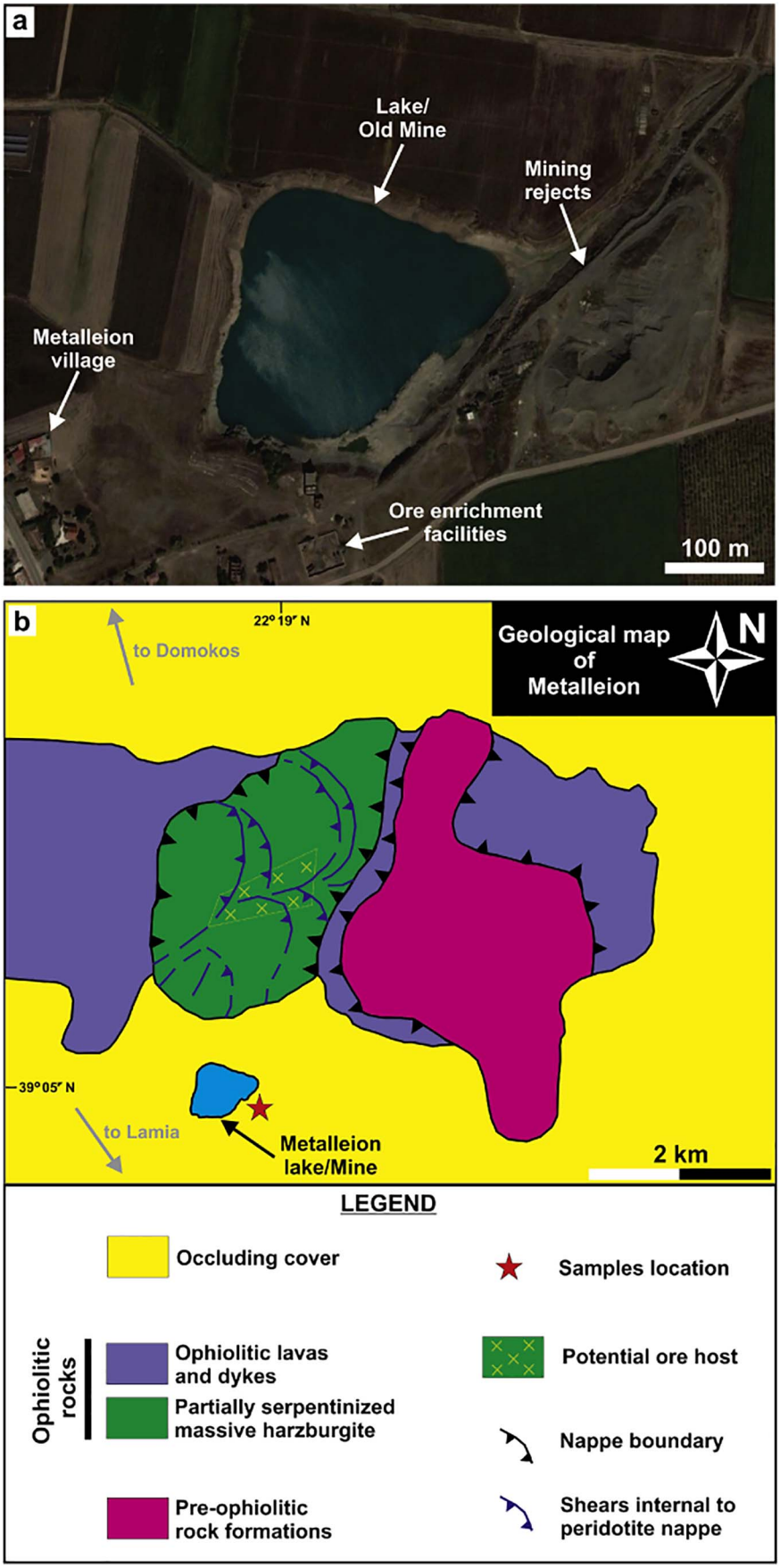

Fig. 3. (a) Aerial photograph of the Metalleion lake (part of the homonymous village can also be seen). The old mine is now underground (beneath the lake). (b) Geological map of the broader Metalleion chrome mine area (Rassios et al., 1991).

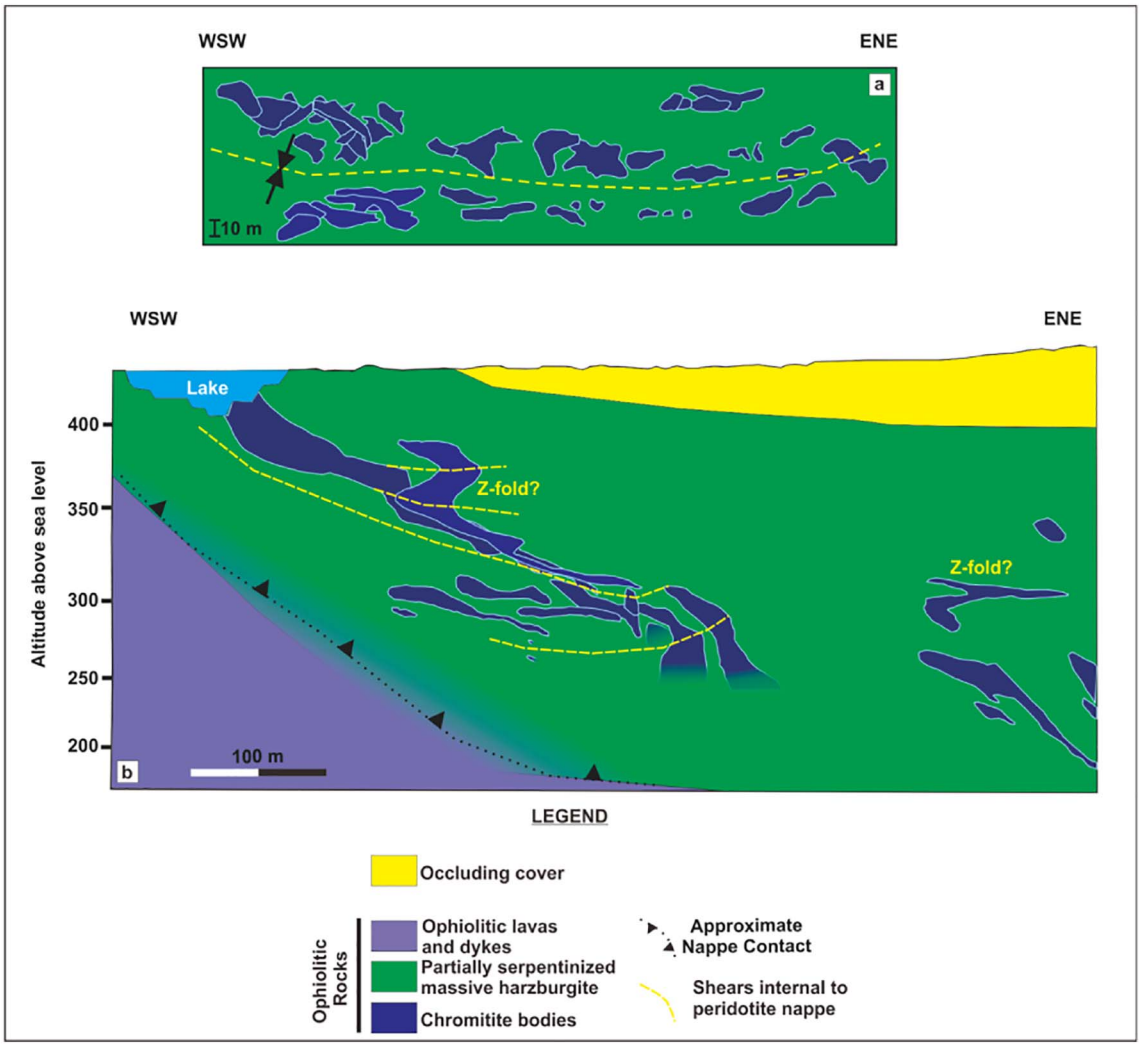

Fig. 4. (a) Planar view of the Metalleion chrome ore bodies over part of the deposits (Hilakos, 1980). (b) Cross-sectional view of the underground distribution of the chrome ore bodies at Metalleion (Psyhogiopoulos, 1985).

measured by LA-ICP-MS using a Resonetics M-50-HR laser coupled with a Thermo-Finnigan® Element 2 at Goethe University, Frankfurt, Germany. The same chromitite mounts used for electron micro-probe analysis (EMPA) were also used here. For each chromitite sample two Cr-spinel crystals were analyzed with one laser spot for the grain core and one for the grain boundary. In addition to the minor element isotopes sought (^{45}Sc, ^{47}Ti, ^{51}V, ^{55}Mn, ^{59}Co, ^{60}Ni, ^{66}Zn and ^{69}Ga), isotopes of other metals (^{25}Mg, ^{29}Si, ^{44}Ca, ^{53}Cr, ^{55}Mn, ^{65}Cu, ^{85}Rb, ^{88}Sr, ^{89}Y, ^{90}Zr, ^{93}Nb, ^{133}Cs, ^{137}Ba, ^{178}Hf, ^{181}Ta, ^{182}W, ^{208}Pb, ^{232}Th, ^{238}U) were monitored during Cr-spinel ablation to constrain the characteristics of the ablated material and check for the possible presence of mineral inclusions. External standardization was achieved using a NIST (National Institute Standards and Technology; Gaithersburg, USA) 612 silicate glass. This glass was used to calibrate the signal, and the quality of calibration was confirmed by re-analysis of NIST 612 after every four shots. The glass was analyzed at the beginning and end of each measurement session, and at regular intervals throughout the session. The data was calibrated to NIST 612 Glass as is common for many geological studies involving LA-ICP-MS analysis. The concentration of ^{25}Mg in Cr-spinel, based on the MgO content earlier determined by EMPA, was used as the internal standard. The signal for each element was normalized to this internal standard correcting for ablation efficiency and instrumental drift. All analyses were done with a spot size of 33 μm, a frequency of 7 Hz, a laser energy density of 90 mJ with a 50% attenuator and 20 demagnification resulting in low fluence (< 2.5 J/cm^2). For each analysis 25–30 s of background was collected (gas blank before firing the laser – these signals were subtracted from the signals measured during analysis) followed by approximately 30 s of sample analysis time (while the laser was firing). Oxide production was minimized to remain below 0.3%. The detection limits are listed in the following as ppm (mg/Kg, 10^{-6} Kg): Ni = 20, Co = 7, V = 30, Zn = 40, Ga = 1, Ti = 35, Sc = 0.5 and Mn = 38. Raw data were processed with the GEMOC GLITTER© software. The resulting precision is better than about 5 to 10% for most elements. Laser ablation-ICP-MS analyses were not performed on ferrian chromite zones due to their limited thickness. Laser ablation data are presented in Table 1.

4. Petrographic description

Chromitites of Metalleion consist of > 85% (modal) coarse-grained Cr-spinel grains. Though it is hard to estimate the exact size of individual Cr-spinel crystals using conventional optical methods, our micro-textural observations show that the largest of them may reach 0.9 mm in diameter. Chromian spinel grains are commonly subhedral to euhedral, but sometimes they may adopt irregular to subrounded crystal habits. Brittle deformation in our samples is expressed in the form of cataclastic compressive fractures that cross cut large Cr-spinels (Fig. 6a) and as long and thick (≤ 0.3 cm) brecciation zones (Fig. 6b).

The intergranular silicate groundmass within the ores is entirely altered to serpentine and chlorite (Fig. 6c). Serpentine shows a typical

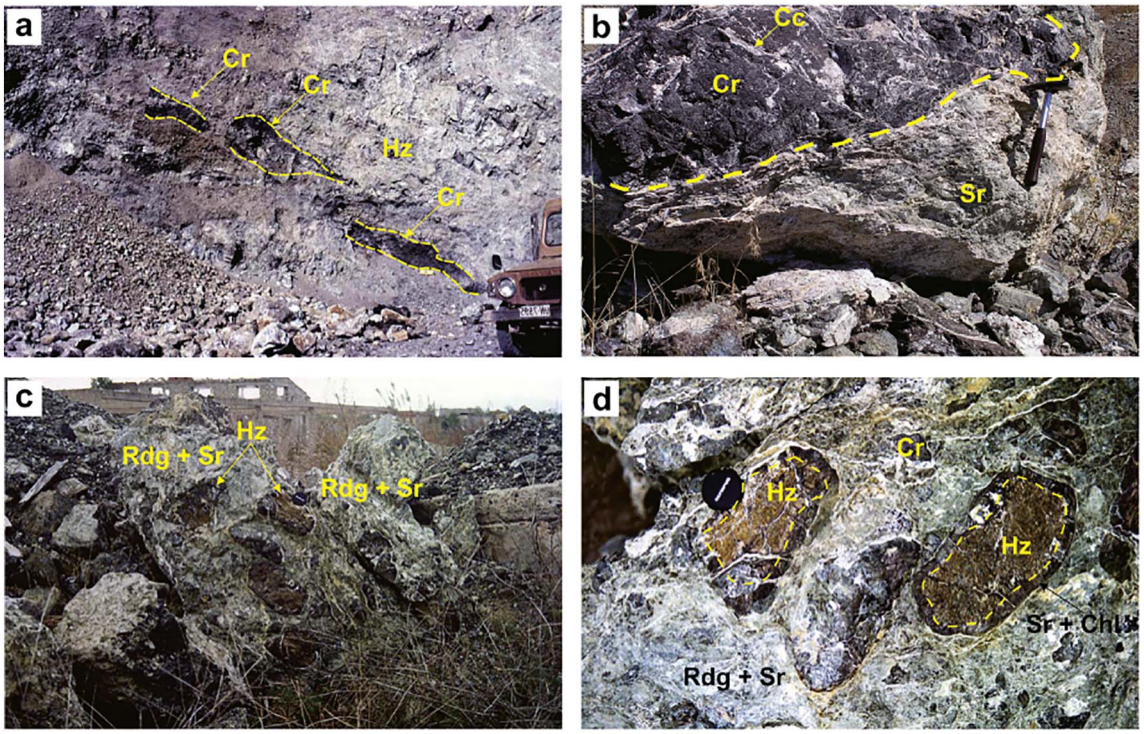

Fig. 5. (a) The Metalleion open pit chrome mine before it was covered by a lake. (b) One of the studied chromitite-peridotite boulders within the quarry talus. Note the contact between chromitite and the host pervasively serpentinized-rodingitized and sheared harzburgite (matrix). (c) A peridotite-ore boulder within the quarry talus. Note that subrounded to egg-shaped blocks of harzburgite and chromitite can still be recognized within a highly pulverized and altered peridotite matrix. (d) Close up of the boulder shown in the previous photo. Note that the peridotite blocks are haloed by cm-scale black-colored reaction rims made up of serpentine ± chlorite and that the matrix is pervasively intruded by thin rodingite microveins. Abbreviations (henceforth in alphabetical order): *Cc* calcite veins, *Chl* chlorite, *Cr* chromitite, *Cpx* clinopyroxene, *Gbr* gabbro, *Hz* harzburgite, *Rdg* rodingite, *Sr* serpentinite, *Srp* serpentine.

Table 1
Minor and trace element concentrations (in ppm) of Cr-spinel (cores and boundaries) from the Metalleion chromitites. All data were acquired by LA-ICP-MS analysis. Chromite composition from the East Pacific Rise MORB and bulk-rock composition of the East Pacific Rise MORB lava are from Pagé and Barnes (2009).

Sample Number	Analysis Number	Isotopes & Detection Limits (in ppm)							
		Sc^{45}	Ti^{47}	V^{51}	Mn^{55}	Co^{59}	Ni^{60}	Zn^{66}	Ga^{69}
		0.5	35	30	38	7	20	40	1
M1	1-core	3.91	416.90	968.24	701.96	146.07	1061.25	474.04	30.69
M1	1-rim	3.50	391.00	912.95	695.82	148.71	1137.29	489.03	31.53
M1	2-core	3.84	414.42	978.50	699.47	148.20	1053.58	500.73	30.47
M1	2-rim	3.74	415.22	973.44	739.76	140.26	1058.13	499.81	32.77
M2	1-core	2.69	438.13	1045.47	779.99	152.67	1226.75	532.34	30.68
M2	1-rim	3.19	415.76	1035.56	813.05	151.40	1340.61	496.45	34.40
M2	2-core	2.61	440.63	1038.78	763.17	149.29	1125.60	509.84	28.54
M2	2-rim	3.91	406.07	1013.12	792.51	147.64	965.90	482.09	32.56
M3	1-core	2.42	334.25	784.65	649.17	138.72	1170.48	442.13	30.06
M3	1-rim	2.49	320.33	783.14	689.17	143.06	1123.51	463.90	29.93
M3	2-core	3.14	348.87	779.66	709.28	135.78	1142.48	439.40	30.03
M3	2-rim	3.32	345.57	799.95	649.88	137.14	1188.70	433.59	30.62
M4	1-core	5.02	344.64	769.06	671.89	137.92	1206.03	431.087	32.16
M4	1-rim	4.80	338.08	792.74	693.41	140.83	1240.73	445.29	32.50
M4	2-core	4.88	325.26	734.22	634.71	131.37	1169.90	424.95	30.46
M4	2-rim	4.92	337.59	770.17	671.45	139.29	1217.66	428.49	31.15
M5	1-core	3.35	445.55	893.70	681.86	142.94	1274.81	488.43	32.95
M5	1-rim	3.18	449.67	908.65	680.49	143.76	1307.69	473.55	32.49
M5	2-core	2.96	439.45	876.57	641.40	142.18	1335.55	468.36	31.63
M5	2-rim	2.83	433.88	887.24	697.14	146.55	1348.66	460.45	31.89
M6	1-core	3.67	347.45	742.95	637.43	135.05	1199.63	400.93	29.59
M6	1-rim	3.53	348.75	761.38	672.35	137.55	1195.95	398.40	29.86
M6	2-core	3.28	350.02	757.16	652.34	138.27	1211.50	428.50	30.76
M6	2-rim	3.06	336.82	733.03	654.17	134.40	1184.80	401.88	29.96
GN10–01/EPR MORB	Chromite	5.3	1343	744	881	165	1766	465	52.5
GN10–01/EPR MORB	Bulk-Rock	29	3977	171	1012	38	565	62	16

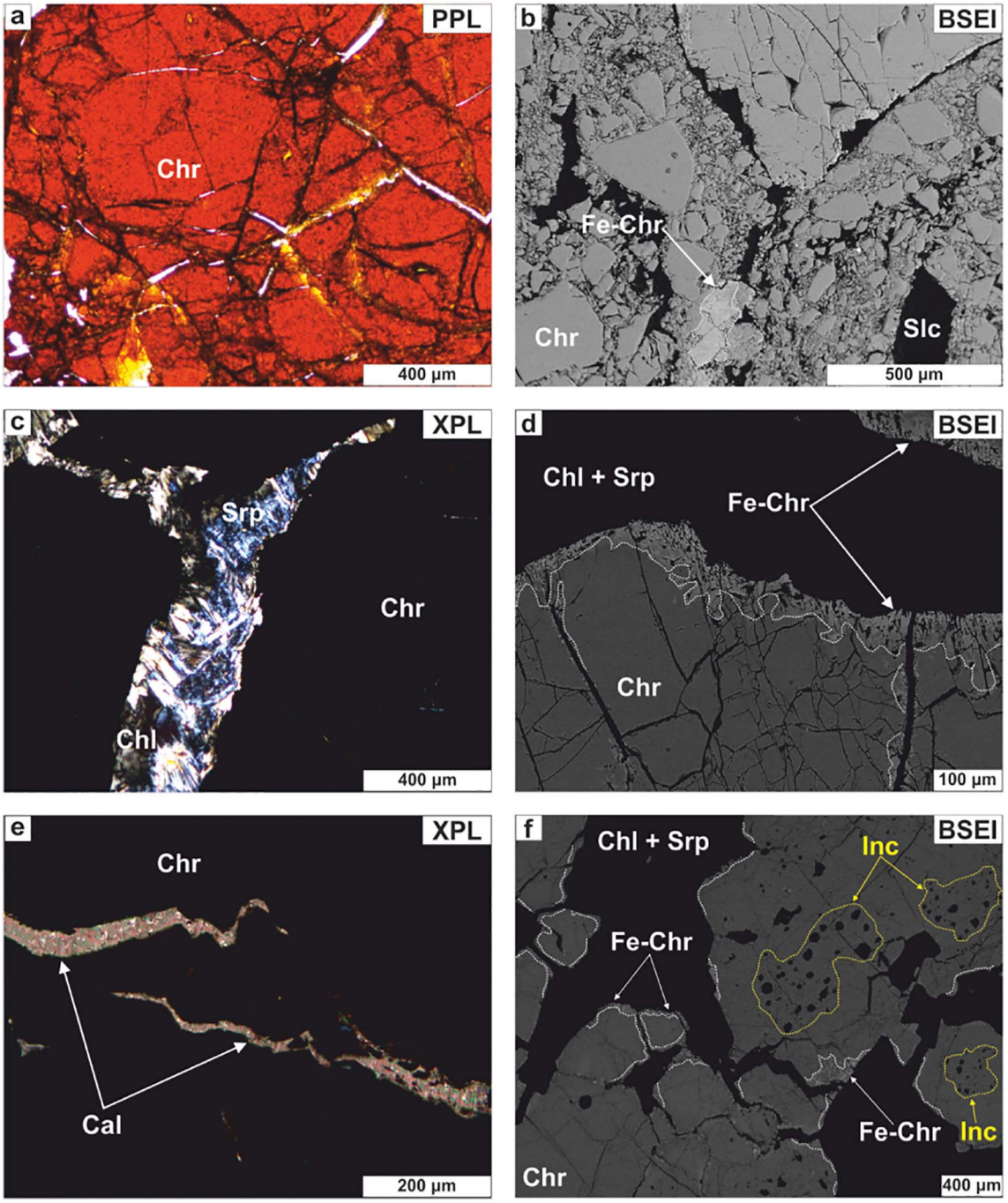

Fig. 6. Chromian spinel grains showing (a) cataclastic texture and (b) strong brecciation. (c) Complete replacement of the interstitial silicate groundmass of chromitites by serpentine and chlorite. (d) Chromian spinel crystals showing limited alteration to ferrian chromite (marked by the white dashed line) across their boundaries. (e) Late calcite microveins cutting Cr-spinel grains. (f) Silicate mineral inclusions distributed in the cores of Cr-spinel grains. Abbreviations [following the system of abbreviations suggested by Whitney and Evans, 2010]: *BSEI* back-scattered electron image, *Cal* calcite, *Chl* chlorite, *Chr* Cr-spinel, *Fe-chr* ferrian chromite, *Inc.* (silicate) inclusions *PPL* plane-polarized (transmitted) light, *Srp* serpentine, *XPL* cross-polarized (transmitted) light. (For interpretation of the references to color in this figure, the reader is referred to the web version of this article.)

pseudomorphic mesh texture after olivine. Non-pseudomorphic serpentine textures (i.e., interlocking and stringy) were also recognized within the Metalleion chromitites. Chlorite blades (≤ 250–300 μm thick) commonly surround Cr-spinel grains forming grey brown to purple intergrowths with serpentine (Fig. 6c). Occasionally serpentine fibers cross cut chlorite, implying their later formation. Petrographic observations show that chlorite is sometimes intergrown with ferrian chromite (≤ 150 μm thick; e.g., Mukherjee et al., 2010) developed along the boundaries (Fig. 6d) and stretching planes of cracked Cr-spinels. Chlorite is also the sole mineral phase filling the pores in ferrian chromite. The boundary between ferrian chromite and the unadulterated Cr-spinel is relatively sharp and easily discernible in back-scattered electron images (BSEI; Fig. 6d).

Late carbonate-bearing microveins (≤ 50 μm thick) are occasionally observed cutting the chromitites (Fig. 6e). Lastly, secondary base metal (BM) minerals such as awaruite and millerite are commonly found dispersed along Cr-spinel cataclastic fractures and brecciation zones.

The Metalleion chromitites contain various types of silicate and metallic minerals as inclusions in Cr-spinel. Any Cr-spinel crystal may contain inclusions, but some individual Cr-spinel grains contain tens of them. In most cases these inclusions are randomly distributed in Cr-spinel, but occasionally they cluster to the core of their host grain

(Fig. 6f). They are mostly anhedral to subrounded/oval in shape indicating that they probably crystallized simultaneously with Cr-spinel (e.g., Xiong et al., 2017 and references therein). They occur as single crystals or polyphase aggregates. The polymineralic inclusions are made up of 2 silicate minerals or combinations of silicates with metallic mineral phases. The size of the silicate inclusions varies from several tens of μm to 400 μm across. The largest of them may communicate with the "outside" world through a network of brittle cracks. Silicate mineral inclusions comprise primary anhydrous [forsterite, enstatite and diopside] and hydrous minerals [edenitic pargasite, phlogopite and aspidolite (the Na-bearing analogue of phlogopite)] with almost no strain; and their altered equivalents (chlorite, serpentine and hydrogrossular). Enstatite intergrown with pargasite is the most common type of composite inclusion. Base metal mineral inclusions are subhedral to euhedral and range in size between 10 and 30 μm. They comprise millerite, chalcopyrite, awaruite and pyrrhotite.

5. Mineral chemistry

5.1. Composition of Cr-spinel in chromitites

5.1.1. Major- and minor-element oxide abundances

The chemistry of Cr-spinel grains from the Metalleion chromitites has been analyzed (sheet 1 in the Supplementary file). Their composition varies in Al_2O_3 (20.03–26.81 wt%), Cr_2O_3 (42.83–51.01 wt%), FeO (10.91–15.23 wt%) and MgO (11.91–16.70 wt%) being comparable to that observed in Cr-spinel from other ophiolitic chromitites (Fig. 7a; Bonavia et al., 1993). The Metalleion chromitites are made up of Cr-spinel with Cr# [Cr/(Cr + Al) × 100] ranging between 53 and 63, Mg# [Mg/(Mg + Fe^{2+}) × 100] varying from 59 to 73 and low Fe^{3+}/ΣFe ratios (≤ 0.28; where ΣFe = Fe^{3+} + Fe^{2+}). Such compositions permit the classification of the investigated chromitites as high-Al or refractory chrome ores ($Cr\#_{Chr}$ < 0.60; Leblanc and Nicolas, 1992).

Minor-element oxide contents in Cr-spinel from the Metalleion chromitites are generally low (TiO_2: ≤ 0.11 wt%, MnO: ≤ 0.20 wt%; sheet 1 in the Supplementary file) as is typical for mantle-hosted ophiolitic chromitites (e.g., Bonavia et al., 1993). However, the V_2O_3 and NiO contents in Cr-spinel from these chromitites are high (V_2O_3 = 0.13–0.26 wt%, NiO ≤ 0.37 wt%; sheet 1 in the Supplementary file). The composition of Cr-spinel from the Metalleion chromitites resembles a lot that of Cr-spinel from the Ayios Stefanos chrome ore bodies (Cr#: 51–66, Mg#: 58–76, Fe^{3+}/ΣFe ≤ 0.28) within the same ophiolite complex (Fig. 2). The only significant difference is the higher TiO_2 content in Cr-spinel from the Ayios Stefanos chromitites (≤ 0.21 wt%; Kapsiotis et al., 2016).

The Cr# and Mg# values of Cr-spinel from the Metalleion chromitites are comparable with those of accessory spinels from mid-ocean ridge basalts (MORB; Dick and Bullen, 1984; Fig. 7b). In the Cr# vs. TiO_2 and Al_2O_3 vs. TiO_2 diagrams (Barnes and Roeder, 2001; Kamenetsky et al., 2001), Cr-spinel analyses from the Metalleion ores plot between the fields of spinels in equilibrium with melts of boninitic and MORB-like affinity (Fig. 7c–d).

Ferrian chromite rims in Cr-spinel show wide variations in Cr_2O_3 (43.99–60.56 wt%), Al_2O_3 (3.12–24.89 wt%), MgO (4.60–16.32 wt%), FeO (8.81–24.08 wt%) and Fe_2O_3 (≤ 6.88 wt%). Furthermore, they exhibit wider variations in Cr# (56–92) and Mg# (27–77) compared to

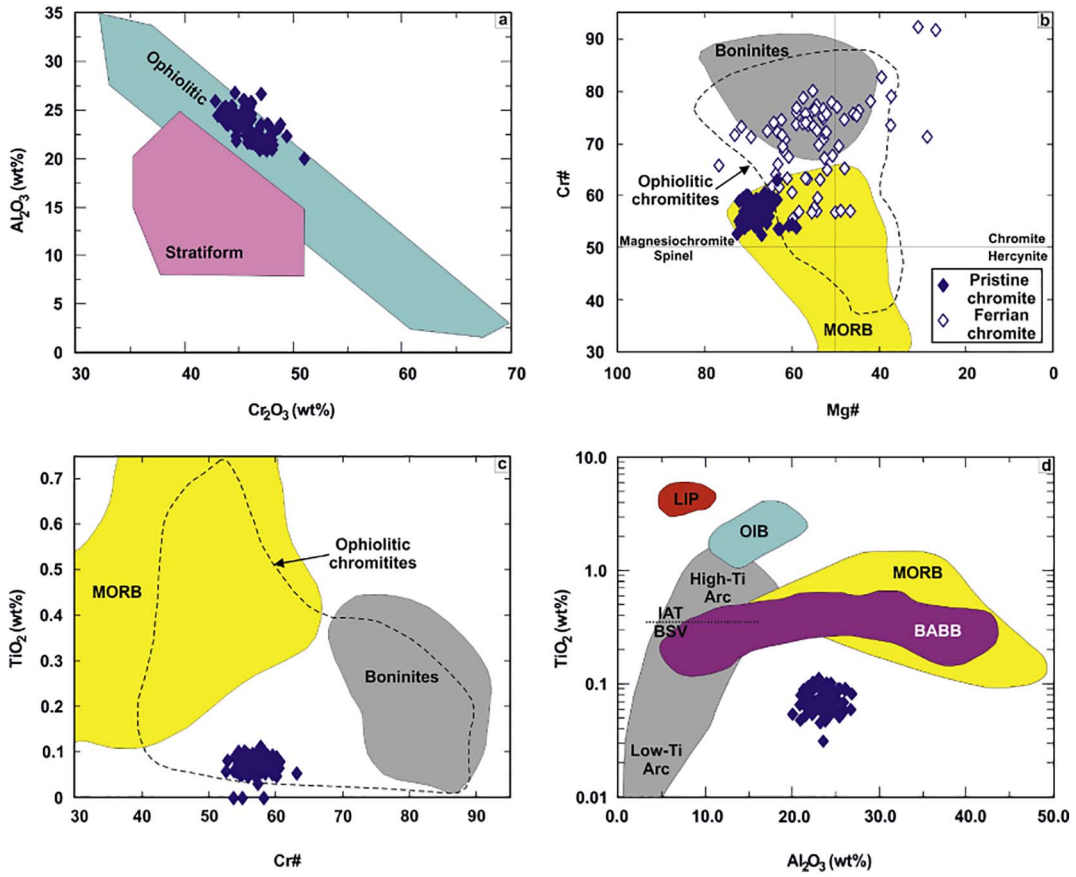

Fig. 7. (a) Al_2O_3 (wt%) vs. chromitites are from Bonavia et al. (1993). (b) Cr# [Cr/(Cr + Al) × 100] vs. Mg# [Mg/(Mg + Fe^{2+}) × 100] plot of Cr-spinel and ferrian chromite analyses from the Metalleion chromitites. Fields for spinel in equilibrium with N-MORBs and boninites are from Dick and Bullen (1984). (c) Composition of Cr-spinel from the Metalleion chromitites plotted on the TiO_2 (wt%) vs. Cr# diagram. All compositional fields are from Barnes and Roeder (2001). (d) TiO_2 vs. Al_2O_3 (wt%) plot of Cr-spinel from the Metalleion chromitites. Compositional fields are from Kamenetsky et al. (2001). Abbreviations: *BABB* back arc basin basalts, *BSV* boninite series volcanics, *IAT* island arc tholeiites, *OIB* ocean islands basalts, *MORB* mid-ocean ridge basalts, *LIP* large igneous province (basalts).

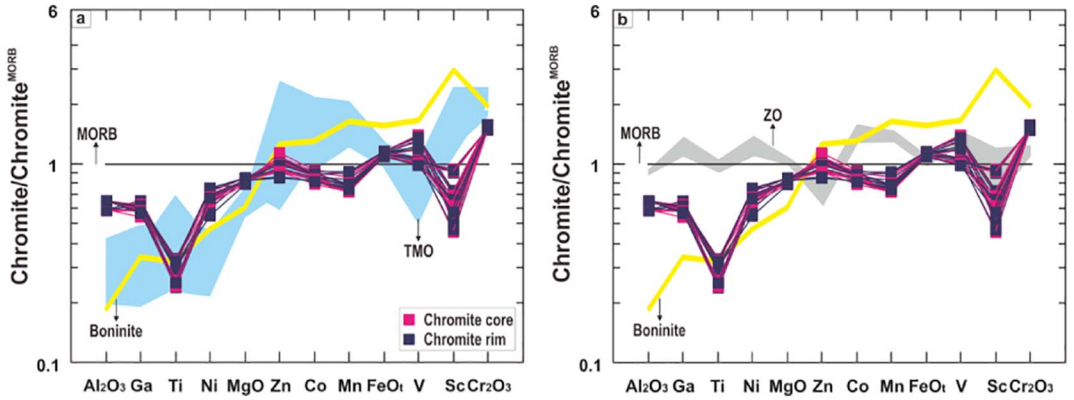

Fig. 8. Profiles of major, minor and trace elements in (unaltered) Cr-spinel from the Metalleion chromitites normalized to the composition of chromite from the East Pacific Rise MORB (Pagé and Barnes, 2009). Data for chromite from the boninite lavas of Bonin Island are from Pagé and Barnes (2009). (a) Data for chromite from the podiform chromitites of the Thetford Mines Ophiolite (*TMO*) crust are also from Pagé and Barnes (2009). (b) Data for chromite from the Al-rich chromitites of the Zambales Ophiolite (*ZO*) are from González-Jiménez et al. (2012).

unaltered Cr-spinel (Fig. 7b) but quite similar $Fe^{3+}/\Sigma Fe$ ratios (≤ 0.31; sheet 2 in the Supplementary file).

5.1.2. Minor- and trace-element contents

Minor- (Ti, Ni, V, Mn and Zn) and trace-element (Sc, Co and Ga) concentrations of Cr-spinel from the Metalleion chromitites are given in Table 1. These LA-ICP-MS analyses were performed on pairs of cores and boundaries of individual Cr-spinel grains to check for any variations in the distribution of elements across the analyzed crystals. These analytical data and the concentrations of some major-element oxides (Al_2O_3, MgO, FeO^{tot}, Cr_2O_3) were normalized to the composition of chromite from the East Pacific Rise MORB (Chr^{MORB}) adapting the normalizing values and order of elements suggested by Pagé and Barnes (2009). We followed this method because in situ LA-ICP-MS analysis of chromite from the East Pacific basalts has shown that it has a homogenous composition characterized by uniform distribution of minor and trace elements. We note that no significant variations in the "topography" of the resultant profiles were observed when normalization was done using the composition of Cr-spinel from primitive mantle or chondrite. Chromian spinel from the Metalleion chromitites has Chr^{MORB}-normalized patterns characterized by negative anomalies in Ti and Sc, and slight positive anomalies in Zn, V and Cr_2O_3 (Fig. 8). Both Cr-spinel cores and boundaries show identical elemental patterns.

Comparison of the contents of minor and trace elements with the average Cr# of Cr-spinels from each chromitite sample shows that the concentrations of V, Mn, Co and Zn decrease with decreasing Cr# (Fig. 9a–c,e), whereas the Ni and Ga contents increase (Fig. 9d,f). These trends are clearly not due to differentiation (e.g., Pagé and Barnes, 2009).

5.2. Composition of minerals in harzburgites

Though the actual scope of this manuscript is to delineate the origin of the chrome ore bodies at Metalleion, a brief report on the composition of minerals in the surrounding harzburgites will aid us to find out if any genetic relation exists between the investigated chromitites and their host rocks.

5.2.1. Primary silicate minerals

Olivine analyses from the Metalleion harzburgites show high forsterite contents [Fo#: $100 \times Mg/(Mg + Fe^{2+}) = 87.7–94.5$]. The NiO content of these olivine grains varies between 0.40 wt% and 0.44 wt%, and the MnO content ranges from 0.12 wt% to 0.14 wt% (sheet 3 in the Supplementary file).

Orthopyroxene from the harzburgites hosting the Metalleion mine is predominantly enstatite with relatively high Al_2O_3 and Cr_2O_3 contents (1.34–2.09 wt% and 0.52–0.63 wt%, respectively; sheet 3 in the Supplementary file). Clinopyroxene is diopside with Mg# values ranging from 93 to 98. The Al_2O_3 and Cr_2O_3 contents of these diopside crystals are low (2.20–2.32 wt% and 0.81–0.88 wt%, respectively; sheet 3 in the Supplementary file).

5.2.2. Chromian spinel

Accessory Cr-spinels in harzburgite have Cr# values that range between 48.39 and 61.43, and Mg# values varying from 56.65 to 63.36. In addition, they are depleted in TiO_2 (≤ 0.06 wt%; sheet 3 in the Supplementary file).

6. Discussion

6.1. Insights into the fate of the dunite sheaths

Old reports and geological observations show that the chromitite-bearing harzburgite at Metalleion is almost barren of dunite (Fig. 5a). However, the presence of chromitites necessitates an origin within a dunite host (e.g., Arai and Miura, 2016 and references therein). If dunite once existed at Metalleion a remaining question could be: how where these ores separated from the dunite? Where the chromitites "squeezed out" of their original dunite sheaths or were their dunite envelopes tectonically eliminated? The original magmatic textures in Cr-spinel within the investigated chromitites have been largely overprinted by mylonitic and brittle deformation. Our observations show that chromitites within some boulders are in immediate contact with a strongly sheared and altered harzburgite matrix (Fig. 5b). This matrix was formed during the entrapment of chromitites in shear zones within the Othris sub-oceanic lithospheric mantle. Relative to chromitite and harzburgite, dunite is a lesser competent material at all *T*. This is because olivine deforms by intracrystalline and annealing mechanisms at *T* wherein harzburgite and chromitite are less easily deformed (harzburgite) or deforming as a brittle substance (chromitite; e.g., Moat, 1986). During high *T* ductile deformation, an apparent thinning of the ductile host around chromitites has been observed in Vourinos, Pindos and Othris. In areas near sub-ophiolitic soles, mylonitic bands of dunite occur within non-mylonitic peridotite host (Rassios et al., 1991). As *T* lessen, dunite within mylonitic zones preferentially accommodates more strain (than harzburgite) due to ease of slip as a result of its monomineralic nature (e.g., Moat, 1986). With even lower *T* but continual shear, dunite forms brittle shear zones, whereas host harzburgite in continuity to these zones is still deforming as a ductile substance. With hydrous penetration, dunite alters to even less competent serpentinite (Grivas et al., 1993). With continuation of shear strain, this ongoing deformation is envisioned to be capable of resulting in almost

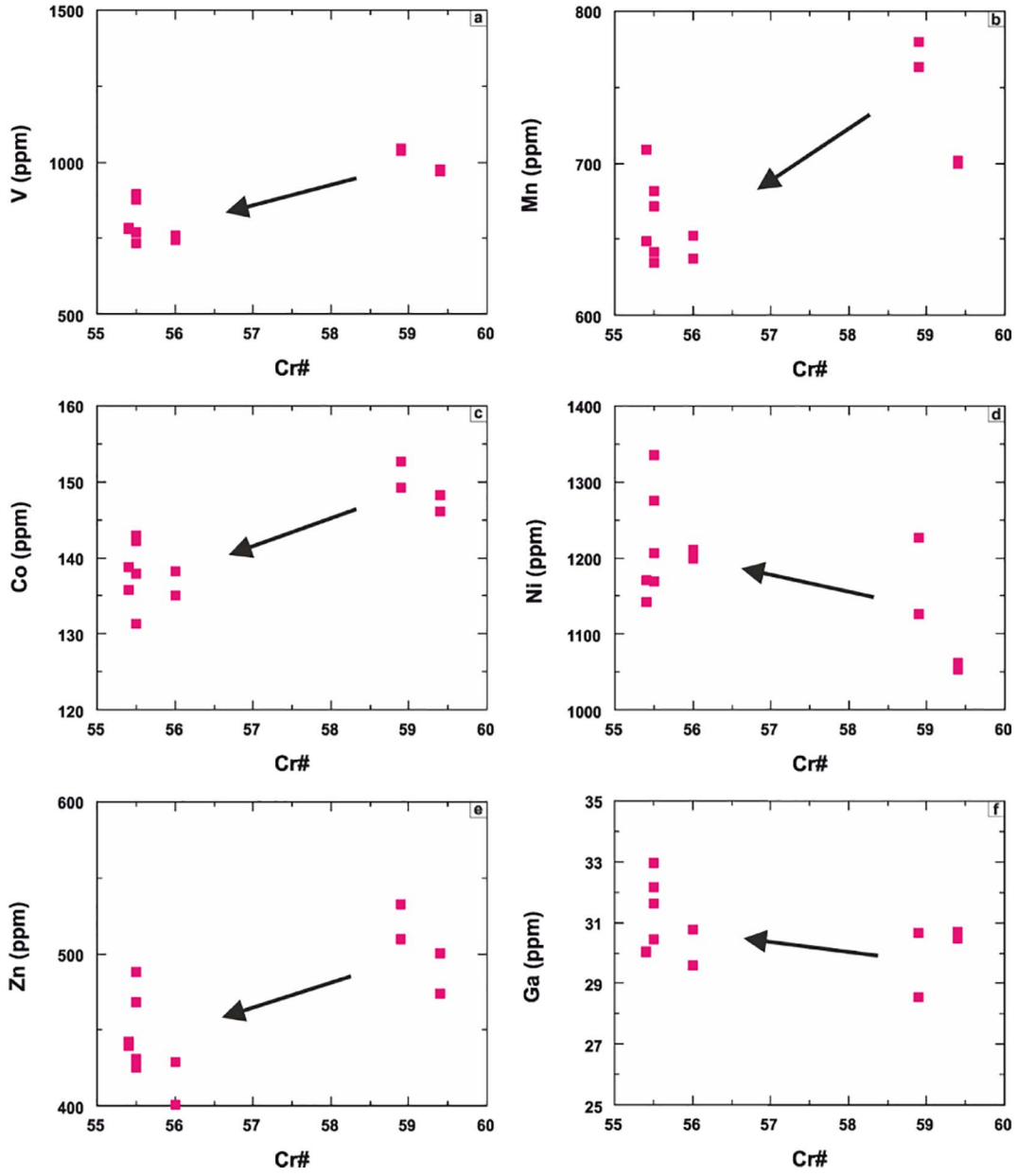

Fig. 9. (a–f) Plots of some minor (Ni, V, Mn and Zn) and trace (Co and Ga) element concentrations vs. the average Cr# of Cr-spinels from the studied chromitite samples (uncertainties are smaller than the symbols size).

complete tectonic obliteration of the original dunite. During this deformation process chromitites behave as rigid bodies rotating in a more ductile peridotite matrix that acts as lubricant as is indicated by the presence of schistose serpentinite in the study area (e.g., González-Jiménez et al., 2016). A similar case is known from the nearby Ayios Stefanos district where Al-rich chromitite pods are sited within a tectonically attenuated dunite-harzburgite thrust zone (Rassios and Konstantopoulou, 1993). However, dunite is still remaining within the Ayios Stefanos thrust zone, which indicates that deformation was more persistent at Metalleion.

We conclude that shearing most likely initiated in ductile conditions, but certainly was active during near-ridgecrest *T* conditions, and continued well into the brittle field. Deformation largely ceased by the time that (undeformed) penetrative rodingite veinlets intruded the pulverized ultramafic matrix (< 400 °C; e.g., Kapsiotis et al., 2017). Even with this speculative range of deforming conditions, it seems clear that the Metalleion ore zone belongs largely to an early phase of the ophiolitic nappe history, presumably when the Othris peridotite nappes were still within an oceanic setting (Rassios et al., in prep.).

6.2. A glance at the cooling history of chromitites

It is widely accepted that pristine Cr-spinel composition evolves via subsolidus exchange of components (re-equilibration) between Cr-spinel and neighboring silicates (e.g., Barnes, 2000) and/or metamorphism (e.g., Grieco and Merlini, 2012). It is also believed that post-magmatic processes have a limited effect on the composition of Cr-spinel within massive chromitites (e.g., Colás et al., 2014). Therefore, it is pertinent to evaluate the impact of any post-magmatic processes on Cr-spinel before the composition of the mineral will be discussed further and implemented to unravel the origin of the Metalleion chromitites.

6.2.1. Compositional variations of major elements in Cr-spinel

Analyses of spinel phases from the massive chromitites of Metalleion show a compositional trend characterized by wide

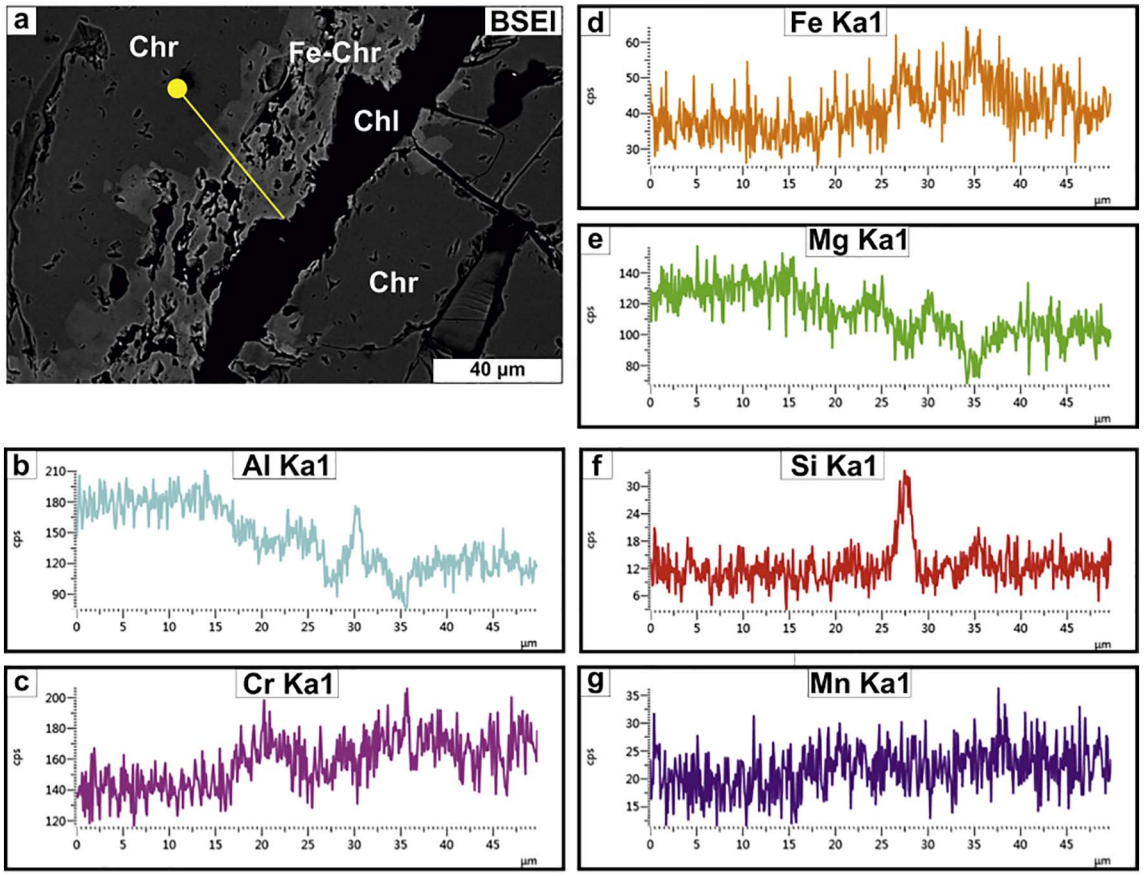

Fig. 10. (a) Back-scattered electron image (BSEI) showing limited peripheral alteration of Cr-spinel to ferrian chromite (abbreviations as in previous figures). (b to g) Single-element (EDS) core-rim profile line scans of Al, Cr, Fe, Mg, Si and Mn demonstrating an (evident) increase in the Fe, Cr and Mn content toward the altered part of the Cr-spinel grain.

variations in Mg# (27–77) and Cr# (53–92; Fig. 7b) at nearly constant Cr-spinel/silicate ratio. It is hard to consider this trend as a result of magmatic differentiation (e.g., Mukherjee et al., 2015 and references therein) or subsolidus re-equilibration between Cr-spinel and neighboring silicates (Kamenetsky et al., 2001; Rollinson et al., 2002). The earliest precipitating Cr-spinel crystals from a fractionating mantle melt would be expected to have high Cr# for high Mg#; this is not the case (Fig. 7b). Furthermore, the nearly monomineralic nature of the Metalleion chromitites precludes the possibility of extensive re-equilibration between Cr-spinel and olivine. This trend of progressive loss of Mg and Al from Cr-spinel coupled with gains in Cr, Fe and Mn (Fig. 10) is due to reaction with olivine in the presence of a post-magmatic fluid (not related to typical serpentinization). This process will eventually result in conversion of Cr-spinel and olivine to ferrian chromite and chlorite, respectively (e.g., Derbyshire et al., 2013).

Ferrian chromite has been viewed as a product of complex metasomatic reactions that are not fully understood yet (e.g., Mellini et al., 2005; Qiu and Zhu, 2017). Though serpentinization is pervasive in the study area, the proportion of ferrian chromite varies among the chromitite samples we examined. This necessitates that chromitites experienced an episode of retrograde (greenschist-facies) metamorphism at reducing conditions as indicated by the low Fe_2O_3 content of ferrian chromite (e.g., Gervilla et al., 2012).

6.2.2. Preservation vs. disturbance of minor- and trace-elements in Cr-spinel

Chromian spinel from the Metalleion chromitites is slightly enriched in Zn and V, and depleted in Ti and Sc (Fig. 8). The minor enrichment in Zn and V is not related to any variations in Mg#; therefore, it cannot be attributed to subsolidus re-equilibration between Cr-spinel and olivine. Another possibility could be that alteration of olivine controls the availability of Zn in the mineralizing fluids (e.g., Gahlan and Arai, 2007). However, such process would lead to a characteristic M-shaped positive anomaly in the segment Zn-Co-Mn of the normalized multi-element patterns (Colás et al., 2014; Fig. 8). This is not what we observe. Colás et al. (2014) concluded that a negative correlation between Zn + Co + Mn and Ga in Cr-spinel at decreasing Mg# could be interpreted as a consequence of amphibolite-facies metamorphism. We notice a positive correlation between Zn + Co + Mn and Ga (Fig. 11). Furthermore, Colás et al. (2014) showed that Ga may be taken up by

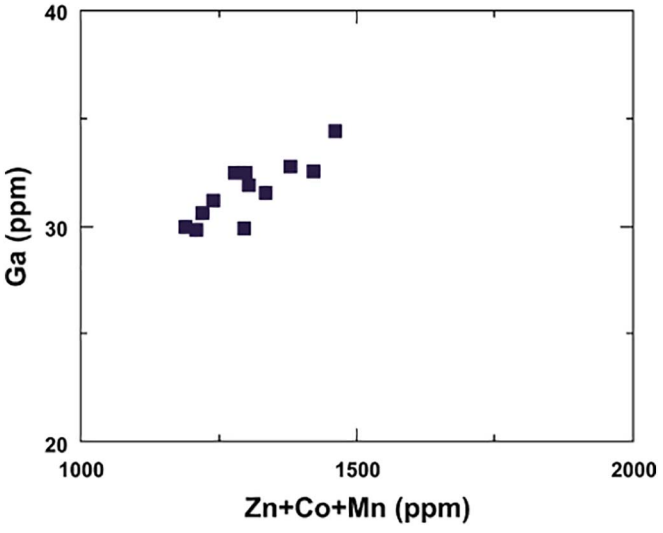

Fig. 11. Ga (ppm) vs. Zn + Co + Mn (ppm) of Cr-spinel cores from the massive chrome ores of Metalleion.

chlorite during metamorphic modification of Cr-spinel. However, there are no significant variations in the contents of Ga between the cores and boundaries of Cr-spinels associated (or not) with chlorite (Table 1). Vanadium, similar to Ga and Ti, does not partition into olivine (Malvin and Drake, 1987; Pagé and Barnes, 2009). This excludes olivine as a potential source for V in Cr-spinel and as a host for Ti. Lastly, depletion in Sc is probably due to the incompatibility of Sc in the lattice of Cr-spinel (e.g., Horn et al., 1994; Righter et al., 2006).

We emphasize that we did not recognize any remarkable differences in the contents of individual minor and trace elements in Cr-spinel from different chromitite specimens (Table 1), though we noticed significant variations in the proportion of chlorite between samples (0–10% modal). The nearly identical Chr^{MORB}-normalized profiles (Fig. 8) imply that minor- and trace-element contents in Cr-spinel were controlled by (a) petrological process(es) that affected all chrome ores in a similar way. Our findings show that minor- and trace-element signatures in Cr-spinel from the Metalleion chromitites can be viewed as intrinsic and identifying igneous features and can be used as proxies to aid us unravel chromitite genesis.

6.3. Parental melt composition

Chromian spinel composition reflects the composition of the primitive melt from which it is an early crystallizing mineral (e.g., Arai, 1992; Barnes and Roeder, 2001). This petrological inference is grounded on studies of massive chromitites as sub-solidus changes in Cr-spinel composition are less apparent in nearly monomineralic chrome ores (e.g., Gervilla et al., 2012). Experimental studies of spinel-liquid equilibrium performed at low P (1 bar) show that the Al_2O_3 content and the FeO/MgO ratio of the parental melt of chromitites can be computed from Cr-spinel composition using the experimental formulae of Maurel and Maurel (1982):

$$(Al_2O_{3Chr}) = 0.035(Al_2O_{3Melt})^{2.42} \quad (1)$$

$$\ln(FeO/MgO)_{Chr} = 0.47–1.07Al\#_{Chr} + 0.64Fe^{3+}\#_{Chr} + \ln(FeO/MgO)_{Melt} \quad (2)$$

where FeO and MgO in wt%, $Al\#_{Chr} = Al/(Cr + Al + Fe^{3+})$ and $Fe^{3+}\#_{Chr} = Fe^{3+}/(Cr + Al + Fe^{3+})$. In addition, the Al_2O_3 and TiO_2 contents of the parental melt of high-Al chromitites can be estimated using the algorithms of Rollinson (2008):

$$(Al_2O_{3Melt}) = 7.1518(Al_2O_{3Chr})^{0.2387} \quad (3)$$

$$(TiO_{2Melt}) = 1.5907(TiO_{2Chr})^{0.6322} \quad (4)$$

which are based on updated datasets of Kamenetsky et al. (2001). We note that TiO_2 and Al_2O_3 concentrations in Cr-spinel cannot be easily perturbed by subsolidus re-equilibration with olivine or post-cumulus reaction with trapped interstitial melt and are directly inherited from the parental magma (Kamenetsky et al., 2001). The implementation of these equations shows that the melt in equilibrium with the Metalleion chromitites had the following composition: 13.79–15.55 wt% and 14.60–15.70 wt% Al_2O_3 applying Eq. 1 and Eq. 3 (Fig. 12a), respectively, ≤ 0.40 wt% TiO_2 (Fig. 12b), and 0.63–1.27 FeO/MgO ratio.

This composition does not resemble that of typical (Phanerozoic) boninites [10.60–14.40 wt% Al_2O_3 (Hickey and Frey, 1982); 11.29–14.87 wt% Al_2O_3 (Falloon et al., 2008)] or back-arc basin basalts (BABB > 16 wt% Al_2O_3; Fryer et al., 1990). In addition, the inferred parental melt of the Metalleion chromitites had a lower TiO_2 content than is typical of MORB (> 0.6 wt% Al_2O_3; Rollinson, 2008). When plotted against the compositions of lavas from the Oman ophiolite the calculated melt compositions straddle the boundaries between the compositional fields of depleted mantle (DM) melts (Schwab and Johnston, 2001; Wasylenki et al., 2003), the low-TiO_2 side of the Lasail and Alley lavas field and the high-Al_2O_3 side of the Alley boninites field (Ishikawa et al., 2002; Fig. 13). Our results show that the parental melt of the Metalleion chromitites was a magma derived from re-melting a depleted mantle source. Could this melt have been a typical island arc tholeiite (IAT)? Chromian spinel composition is against this scenario (Fig. 7c–d). Furthermore, the highly depleted-in-TiO_2 nature of Cr-spinel discards the possibility that a MORB-like magma [i.e., forearc basalt (FAB; Reagan et al., 2010; Ishizuka et al., 2011)] was involved in the formation of the Metalleion chrome ores.

Clearly the genesis of these chromitites must be attributed to a special type of melt with transitional compositional signatures between those of MORB/FAB, IAT and boninites (Figs. 7b–d, 8). Basalt blocks with intermediate affinity between MORB and IAT [known as medium-Ti basalts (MTB)] have been reported from the Agoriani mélange in West Othris (Photiades et al., 2003). However, these lavas represent nearly primitive melts that have not experienced significant fractionation en route to the crust as indicated by the relatively limited variation in their bulk-rock Mg# (76–61; Saccani et al., 2011; E. Saccani, Personal communication). None of the known lavas from Othris could be considered as the volcanic equivalent of the parental magmas of the Metalleion chromitites. This petrological “gap” may be due to sampling bias or it might be indicating that after the formation of chromitites the resultant melts cooled rapidly on their ascent through the uppermost mantle. The wide range of geochemical affinities presented by the Othris volcanic rocks (Saccani, 2015) make the possibility of melt stagnation within the lithospheric mantle hard to accept.

It is quite intriguing that the most significant chrome ore occurrences in Othris (Ayios Stefanos, Eretria and Metalleion) are Al-rich. Experimental work and geological evidence support that high-Cr chromitites form mainly in settings of harzburgite-boninite melt interaction (e.g., Zhou et al., 1996). Boninites are known from Othris (Vrinena and Aerino; Koutsovitis and Magganas, 2016). Therefore, a legitimate question could be: why are high-Cr chromitites missing from Othris? Different hypotheses could explain the absence of large-scale interaction between boninitic magmas and harzburgites in the Othris lithospheric mantle. One scenario would involve rapid extension of an accreted oceanic lithosphere horizontally away from the magma-rich region of a forearc spreading center at an advanced stage of slab subduction (e.g., Xiong et al., 2017). An alternative hypothesis necessitates the release of limited volumes of boninite melts from the Othris mantle. Possible support for this scenario arises from the documentation of scarce boninite veins (< 40 cm thick; P. Koutsovitis, Personal communication) intruding the host peridotites (Koutsovitis and Magganas, 2016).

6.4. Hints on the mantle melting conditions

Our calculations show that the parental melts of the Metalleion chromitites were produced by re-melting of a depleted mantle source. We note that these melts have nearly invariable Al_2O_3 and TiO_2 concentrations (Fig. 13), which is quite important as it implies a narrow variation in the degree of melting of their mantle source (e.g., Pearce et al., 2000). Furthermore, the parental melts of the investigated chromitites have high Al_2O_3 concentrations (14.60–15.70 wt%), indicating that they derived from melting of a relatively fertile mantle source (e.g., Kamenetsky et al., 2001; Rollinson and Adetunji, 2015). We emphasize that a MORB-depleted (clinopyroxene-bearing) harzburgite could be the conceivable source of the parental melts of the Metalleion chromitites. However, dry melting of depleted harzburgite would require an anomalously high thermal regime (e.g., Bébien et al., 2000; Saccani, 2015). In contrast, water is known to increase the degree of partial melting by lowering peridotite solidus (e.g., Green, 1976; Mysen and Kushiro, 1977). The presence of primary hydrous silicate mineral inclusions in Cr-spinel indicates that the Metalleion chromitites were formed by a water-bearing magma (e.g., Johan et al., 1983; Matveev and Ballhaus, 2002) produced by wet mantle melting.

Water is also known to increase the oxidation status of a melt (Feig et al., 2006). The concentration of V in Cr-spinel is greatly influenced

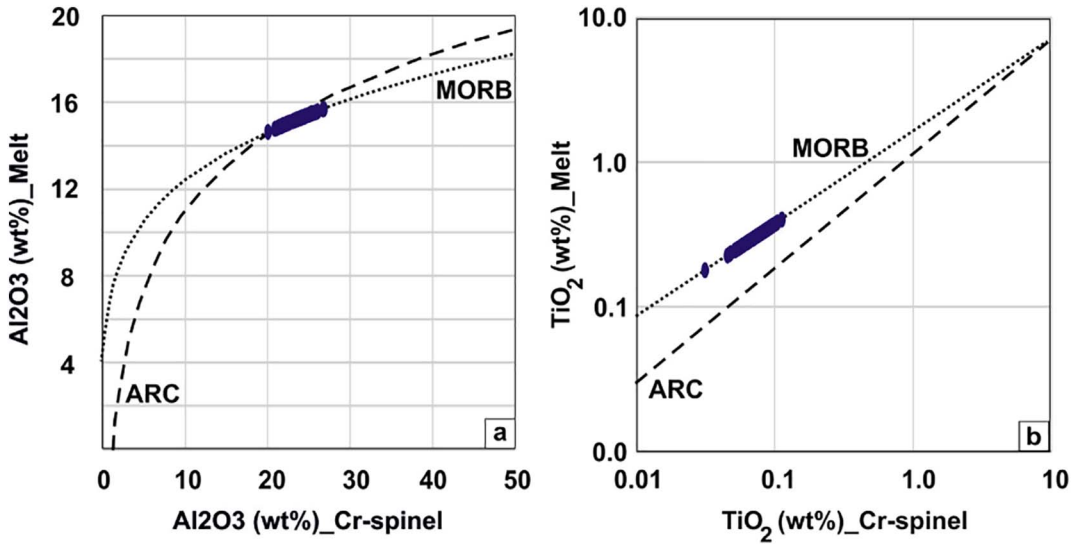

Fig. 12. Plots of (a) Al_2O_3 and (b) TiO_2 calculated to model parental melts in equilibrium with the Metalleion chromitites. The MORB and Arc lines are from Rollinson (2008).

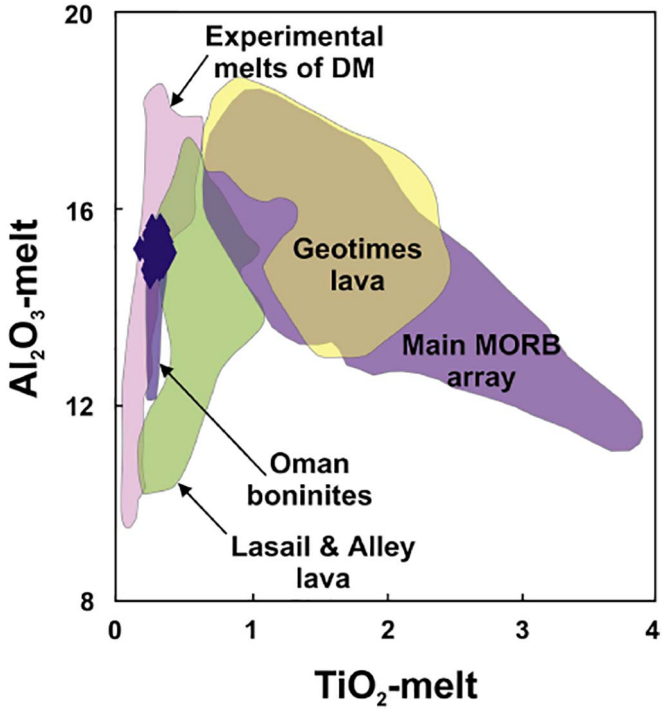

Fig. 13. Calculated parental melt compositions for the Metalleion chromitites relative to the compositional fields for experimental depleted melts (Schwab and Johnston, 2001; Wasylenki et al., 2003), MORB lavas, boninites (Ishikawa et al., 2002) and lava units from the Oman ophiolite (after Rollinson, 2008).

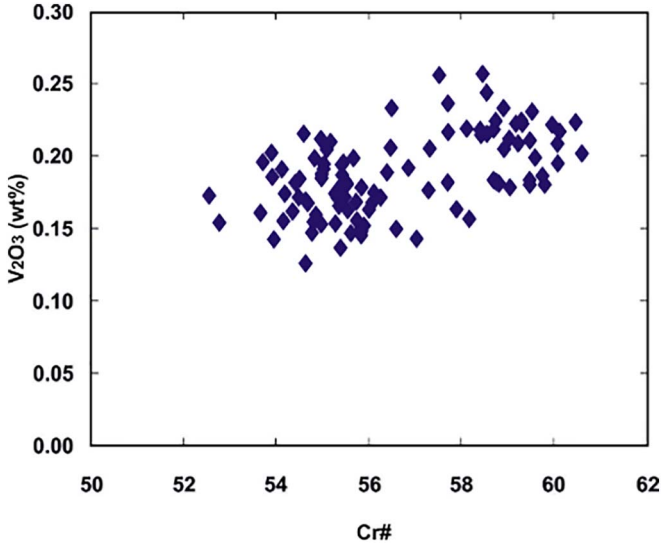

Fig. 14. V_2O_3 (wt%) vs. Cr# of Cr-spinel from the Metalleion chromitites.

by the degree of oxidation of magma. As melt fractionation proceeds a magma will become more oxidized and the concentration of V in Cr-spinel will be expected to increase (e.g., Pagé and Barnes, 2009). However, what we note here is that V_2O_3 is positively correlated with Cr# (Fig. 14). It is intriguing that this is also the situation for Mn and Zn. The concentrations of these elements are positively correlated with Cr# (Fig. 9b,e). This indicates that the compatibility of V^{3+}, Mn^{2+} and Zn^{2+} in Cr-spinel was initially high in a magmatic system characterized by high but gradually declining fO_2 (Horn et al., 1994; Canil, 1999) or water concentration (Pagé and Barnes, 2009). The distribution of primary hydrosilicates in the core of the Cr-spinel host indicates that the concentration of water in the melt was progressively decreasing during the genesis of the investigated chromitites.

Our findings indicate that the parental melts of the Metalleion chromitites originate from a hydrated and oxidized MORB-depleted harzburgite source. This type of peridotite is quite common in the Othris mantle section (e.g., Barth et al., 2008). A similar conclusion has been reached for the chromitites of the Ayios Stefanos district (West Othris). These chromitites consist of Cr-spinel with a higher TiO_2 concentration than that of Cr-spinel from the chrome ores of Metalleion (Kapsiotis et al., 2016). This implies that the Othris chromitites derive from geochemically and spatially distinct melt inputs generated by melting of a heterogeneously depleted mantle (González-Jiménez et al., 2011).

6.5. *Putting melt-peridotite interaction to the test*

A critical aspect of all contemporary models for the genesis of ophiolitic chromitites involves interaction between mafic melts migrating through the upper mantle and harzburgite, followed by mixing of melts of different origins and degrees of fractionation at the intersection between porous dunite channels (González-Jiménez et al., 2014 and references therein). During harzburgite-melt interaction orthopyroxene dissolution promotes harzburgite replacement by dunite along

the interaction wall, which explains why chromitites are commonly enveloped by dunites (e.g., Quick, 1981; Zhou et al., 1994).

The Metalleion chromitites are out of immediate contact with a dunite host. This brings into question the validity of melt-peridotite interaction as the appropriate mechanism for their genesis. Nevertheless, a number of findings indicate that this petrological process controlled the formation of chromitites at Metalleion. These chromitites are found in depleted harzburgites containing pyroxenes with relatively high Al (Al_2O_{3Opx} = 1.34–2.09 wt%, Al_2O_{3Cpx} = 2.20–2.32 wt%) and Cr contents (Cr_2O_{3Opx} = 0.52–0.63 wt %, Cr_2O_{3Cpx} = 0.81–0.88 wt%) and accessory Cr-spinel with Cr# ranging between 48 and 63 (sheet 3 in the supplementary file). Such type of harzburgite is supposed to be an ideal source for the amount of Cr and Al required for chromitite formation via harzburgite-melt interaction followed by melt mixing (Arai, 1997). The similarity in the Cr# of Cr-spinel between chromitites and harzburgites implies that chromitites have reached equilibrium with ambient harzburgite via involvement of a melt (Arai and Miura, 2016). It also indicates that melt-rock reaction did not happen far away from the mantle level where the chromitites were originally emplaced. This is also corroborated by the low TiO_2 content of the parental melts of chromitites (≤ 0.40 wt%) indicating that these magmas were not significantly modified by metasomatism during their ascent through the mantle (e.g., Rollinson and Adetunji, 2015).

We note the absence of a super-reducing ultra-high pressure (SuR-UHP) mineral assemblage in the chromitite samples we examined. We also emphasize that we did not observe any equilibration microstructures in Cr-spinel such as coarse Cr-spinel grains with diopside exsolution lamellae that could be inherited from a pre-existing high-*P* spinel polymorph [i.e., Ca-Ferrite ($CaFe_2O_4$); e.g., Xiong et al., 2017]. These features rule out the possibility that the investigated chromitites were subducted deep into the upper mantle and then rapidly exhumed back to shallow mantle levels (e.g., Zhou et al., 2014). We, however, note the coexistence of pargasitic amphibole, aspidolite and serpentine within Cr-spinel from the Metalleion chrome ores. This petrographic observation indicates rapid cooling from the Cr-spinel liquidus *T* (~1250 ± 100 °C at < 1.5 GPa; e.g., Feig et al., 2006) down to the maximum stability *T* for Na-bearing amphibole and aspidolite (lower than 1050 °C at ~1–2 GPa; Wendlandt and Eggler, 1980; Niida and Green, 1999), and serpentine (~720 °C and 2.0 GPa; Ulmer and Trommsdorff, 1995). These *P-T* conditions are in accordance with the proposed scenario for the genesis of the Metalleion chromitites; that is, large-scale interaction of high-*T* primitive magmas (released from a hydrated and oxidized MORB-depleted source) with low-*T* depleted harzburgites at shallow mantle levels during continuous cooling (from ~1000–1100 to ~700 °C) and subsequent (primitive) melt-(evolved) melt mixing (e.g., Xiong et al., 2017).

6.6. Geotectonic setting

The Othris ophiolite contains a diverse suite of mantle peridotites (plagioclase-bearing lherzolites, amphibole- and plagioclase-bearing harzburgites, lherzolites, harzburgites and dunites; Menzies, 1973; Dijkstra et al., 2001) indicative of both MOR- and SSZ-type settings (Barth et al., 2008). On the basis of a compositional study of pyroxenes Bizimis et al. (2000) concluded that the East Othris peridotites originated in a SSZ environment. Furthermore, Barth et al. (2008) noted that abyssal-type peridotites dominate in Fournos Kaïtsa and western Katáchloron, whereas MOR- and SSZ-type peridotites coexist in eastern Katáchloron, Metalleion-Domokos and Eretria. This lithological coexistence was ascribed to localized flux of a slab-derived fluid to the Othris mantle during a stage of melting in a SSZ setting. It was suggested that Othris represents a transient phase of subduction initiation at (or near) a MOR. However, based on micro-structural and petrological studies Dijkstra et al. (2001, 2003) argued that the West Othris Peridotite Massif resembles sub-oceanic mantle from a near-transform fault region of a slow-spreading, Atlantic-type MOR. This transform fault might be related to the early dismemberment of the West Othris peridotites into a series of ultramafic nappes (Rassios and Konstantopoulou, 1993).

The Domokos peridotite nappe cropping out < 1 km north of the Metalleion mine (Fig. 3b) has long been assumed to be continuous (beneath the sedimentary cover) with the harzburgites of the mine itself. A structural reconnaissance shows that this peridotite nappe is divided into two parts by a relatively narrow and shallow *E*-W trending depression filled with recent alluvia. These alluvia deposits follow and cover the trace of a fault structurally delineated by the sheared contacts of several internal imbricates verging to the E (Fig. 3b); these define a minor strike-slip tear fault system. Intriguingly, this fault does not penetrate into the non-ophiolitic rock units beneath or adjacent to the peridotite nappe. This implies the oceanic origin of the fault. We note the existence of trivial refertilized peridotites (plagioclase-bearing harzburgites) and basaltic intrusions of varying degree of deformation and dual geochemical affinity [boninitic (TiO_2 = 0.3 wt%, V = 282.6 ppm; Unpubl. data) and MORB (TiO_2 = 2.9 wt%, V = 499.3 ppm; Unpubl. data); e.g., Shervais, 1982] within the Metalleion-Domokos peridotite nappe. All these could be identifying aspects of a peridotite body from a transform fault-related oceanic region (e.g., Bonatti et al., 1992; Cannat et al., 1992; Constantin, 1999). Field observations imply that the Domokos fault mechanically milled the chrome ores to their present state (Fig. 5c–d). Consequently, the question arises as to whether the Domokos “fossil” oceanic fault is related to the genesis of the Metalleion chromitites.

6.6.1. Where did the Metalleion chromitites form?

Geochemical calculations demonstrate that the parental melts of chromitites at Metalleion had intermediate affinity between MOR- and arc-derived magmas. Petrologic estimations predict the genesis of such magmas in the mantle beneath back-arc basins (BAB). However, it is unlikely that the Othris ophiolites formed in a BAB (Barth et al., 2008). Diorites and pyroclastic rocks that could point toward a pre-existing mature intra-oceanic arc have never been reported from Othris (Barth et al., 2008). Moreover, a spatial association of Cr-rich and Al-rich chromitites that could be indicative of a mature forearc/arc setting is missing from Othris.

The low Cr# and high Ga content of Cr-spinel from the Metalleion chromitites (Fig. 9f) necessitates parental magma genesis by hydrous melting of an oxidized mantle source that had previously experienced melting in a MOR regime (e.g., Alabaster et al., 1982; Dare, 2007; Pagé and Barnes, 2009). This could reflect an asthenospheric melting regime influenced at some extent by a subduction component derived from a downgoing lithospheric slab (e.g., Rollinson and Adetunji, 2015). This is possible to happen during subduction initiation when asthenosphere rises to fill the “gap” created by the early sinking of a descending lithospheric slab (e.g., Stern et al., 2012 and references therein).

Considering the scale of the mine's dimensions, the chrome ore zone can be best described as the remnant of a large WSW–ENE-oriented ductile-brittle shear zone (Psyhogiopoulos, 1985; Fig. 4b) that correlates with the transforming direction of the Domokos fault (Rassios and Konstantopoulou, 1993). The chromitites themselves are highly deformed and constrained in location to that fault zone. This zone started deforming at high *T* and was internally dismembered to a mixture of chromitite and peridotite blocks within a pulverized ultramafic matrix much resembling a fault breccia (Fig. 5c–d). This pulverized lithology is similar to the fine-grained rock powder aiding dynamic unstable slip over a fault plane known in the geological literature as gouge (e.g., Reches and Lockner, 2010).

Our preferred hypothesis for the origin of the Metalleion chromitites is that they record a stage of magmatism at or close to the junction between a near-transform fault and the upper slab of an infant intra-oceanic subduction zone near an active MOR (Fig. 15a). A similar case of chromitites formation in a proto-forearc setting where hot

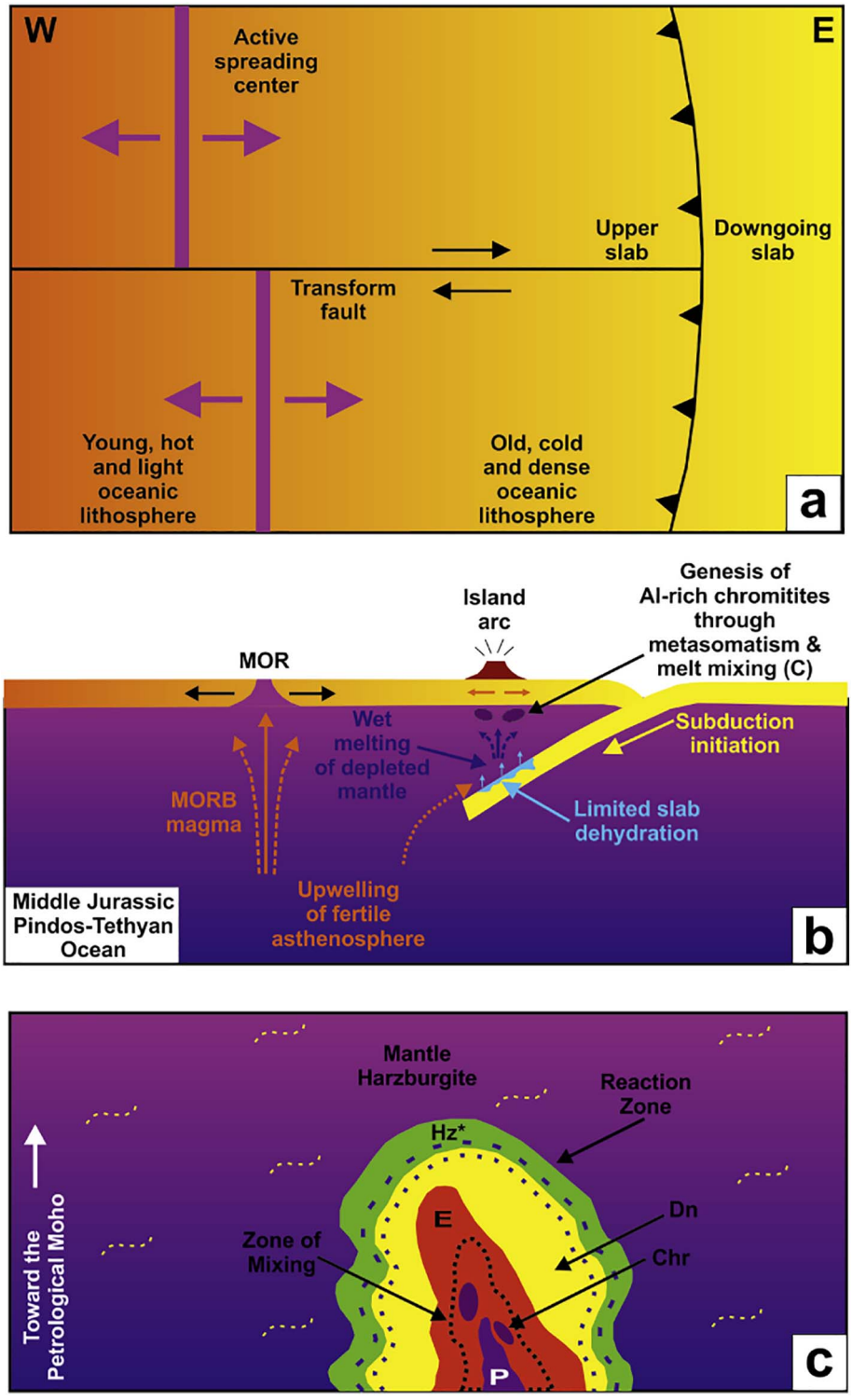

Fig. 15. Schematic cartoon illustrating the geotectonic setting of the Metalleion refractory chromitites. (a) A transform fault links together a spreading center and the upper block of an immature subduction zone during the beginning of the closure of the Neotethyan Pindos Ocean (bird's eye view). (b) Early subsidence of old, cold and dense oceanic lithosphere allows asthenosphere to start flowing below a near-transform fault ending at the upper slab of an infant intra-oceanic subduction zone (cross section). In this melting regime upwelling asthenospheric melts will be progressively influenced by a subduction component from a descending lithospheric slab. (c) Mantle harzburgite is metasomatically replaced by dunite. Chromitites will precipitate from hybridized melts generated by mixing of evolved melts and primitive melts within small dunite conduits. Foliation is shown by dotted wavy yellow lines. Abbreviations: *Chr* chromitite, *Dn* dunite, *E* evolved melt, *Hz* harzburgite, *Hz** harzburgite with low orthopyroxene content, *P* primitive melt. (For interpretation of the references to colour in this figure legend, the reader is referred to the web version of this article.)

asthenospheric melts rose along a transform fault during subduction instigation has been reported from the Poum massif, New Caledonia ophiolite (Leblanc, 1995; Malpas et al., 1997). We emphasize that the transform fault deformed primarily around the chromitites because the ore bodies were more competent and served as breaking-points in the deforming system. However, it is not clear if the ores precipitated from a melt intruding the transform fault or if the chromitites were pre-existing the transform fault and mushed together to form massive ore bodies in the context of a deforming process facilitated by the transform fault. Though it is not easy to provide a direct answer to this causality dilemma we are in favor of the first option. The main reason for this is that in a setting where plate subduction is initiated below a transform fault zone hot asthenosphere must rise to fill the resultant "gap" (Fig. 15b; e.g., Zhang et al., 2016). This process will trigger extensive wet melting of depleted mantle producing primitive magmas that will be modified through harzburgite-melt interaction at shallow mantle levels. Mantle metasomatism will promote harzburgite replacement by dunite along the interaction wall (Fig. 15c). Mixing of the modified melt with the next pulse of primitive magma within dunite will trigger saturation of the resultant (hybridized) melt in Cr-spinel and eventually

the formation of chromitites (Fig. 15c; e.g., Arai and Yurimoto, 1994; Zhou et al., 1994, 1996).

7. Concluding remarks

1. The Metalleion chromitites are out of immediate contact with dunite owing to immense shearing that resulted in almost complete tectonic obliteration of their host dunites.
2. These are massive and high-Al ore pods containing Cr-spinel (Cr# = 53–63) slightly rich in V and Zn, but poor in Ti and Sc compared to Cr-spinel from typical MORB and boninite lavas.
3. The parental magmas of these chromitites were generated by hydrous melting of an oxidized and heterogeneously depleted mantle (DM) source.
4. The genesis of chromitites is envisioned to have occurred via melt-harzburgite interaction followed by (primitive) melt-(evolved) melt mixing beneath an infant forearc basin linked to a nearby MOR with a transform fault.

Acknowledgements

We would like to express our sincere gratitude to Dr. Robert Ayuso, Editor-in-Chief of Journal of Geochemical Exploration, for the editorial handling of this paper. We are also grateful to two anonymous reviewers for their constructive feedback and helpful comments, which greatly improved an earlier version of our manuscript. Research was partly supported by the National Natural Science Foundation of China (NNSFC; Youth Science Fund Project No. 41402065) and Sun Yat-sen University Special Fund Project (Young Faculty's Research Start-up Grant No. 32110-31121401).

Conflict of interest

The authors declare that they have no conflict of interest.

Appendix A. Supplementary data

Supplementary data to this article can be found online at https://doi.org/10.1016/j.gexplo.2017.11.003.

References

Alabaster, T., Pearce, J.A., Malpas, J., 1982. The volcanic stratigraphy and petrogenesis of the Oman Ophiolite Complex. Contrib. Mineral. Petrol. 81, 168–183.
Arai, S., 1992. Chemistry of chromian spinel in volcanic rocks as a potential guide to magma chemistry. Mineral. Mag. 56, 173–184.
Arai, S., 1997. Control of wall-rock composition on the formation of podiform chromitites as a result of magma/peridotite interaction. Resour. Geol. 47, 177–187.
Arai, S., Miura, M., 2016. Formation and modification of chromitites in the mantle. Lithos 264, 277–295.
Arai, S., Yurimoto, H., 1994. Podiform chromitites of the Tari–Misaka ultramafic complex, Southwest Japan, as mantle–melt interaction products. Econ. Geol. 89, 1279–1288.
Arai, S., Uesugi, J., Ahmed, A.H., 2004. Upper crustal podiform chromitite from the northern Oman ophiolite as the stratigraphically shallowest chromitite in ophiolite and its implication for Cr concentration. Contrib. Mineral. Petrol. 147, 145–154.
Barnes, S.J., 2000. Chromite in Komatiites, II. Modification during greenschist to mid-amphibolite facies metamorphism. J. Petrol. 41, 387–409.
Barnes, S.J., Roeder, P.L., 2001. The range of spinel compositions in terrestrial mafic and ultramafic rocks. J. Petrol. 42, 2279–2302.
Barth, M.G., Mason, P.R.D., Davies, G.R., Dijkstra, A.H., Drury, M.R., 2003. Geochemistry of the Othris Ophiolite, Greece: evidence for refertilization? J. Petrol. 44, 1759–1785.
Barth, M.G., Mason, P.R.D., Davies, G.R., Drury, M.R., 2008. The Othris Ophiolite, Greece: a snapshot of subduction initiation at a mid-ocean ridge. Lithos 100, 234–254.
Bébien, J., Dimo-Lahitte, A., Vergély, P., Insergueix-Filippi, D., Dupeyrat, L., 2000. Albanian ophiolites. I – magmatic and metamorphic processes associated with the initiation of a subduction. Ofioliti 25, 39–45.
Bizimis, M., Salters, V.J.M., Bonatti, E., 2000. Trace and REE content of clinopyroxenes from supra-subduction zone peridotites. Implications for melting and enrichment processes in island arcs. Chem. Geol. 165, 67–85.
Bonatti, E., Peyve, A., Kepezhinskas, P., Kurentsova, N., Seyler, M., Skolotnev, S., Udintsev, G., 1992. Upper mantle heterogeneity bellow the Mid-Atlantic Ridge, 0°–15° N. J. Geophys. Res. 97, 4461–4476.
Bonavia, F.F., Diella, V., Ferrario, A., 1993. Precambrian podiform chromitites from Kenticha Hill, Southern Ethiopia. Econ. Geol. 88, 198–202.
Canil, D., 1999. Vanadium partitioning between orthopyroxene, spinel and silicate melt and the redox states of mantle source regions for primary magmas. Geochim. Cosmochim. Acta 63 (3–4), 557–572.
Cannat, M., Bideau, D., Bougault, H., 1992. Serpentinized peridotites and gabbros in the Mid-Atlantic Ridge axial valley at 15°37′N and 16°52′N. Earth Planet. Sci. Lett. 109, 87–106.
Colás, V., González-Jimenéz, J.M., Griffin, W.L., Fanlo, I., Gervilla, F., O'Reilly, S.Y., Pearson, N.J., Kerestedjian, T., Proenza, J.A., 2014. Fingerprints of metamorphism in chromite: new insights from minor and trace elements. Chem. Geol. 389, 137–152.
Constantin, M., 1999. Gabbroic intrusions and magmatic metasomatism in harzburgites from the Garrett transform fault: implications for the nature of the mantle–crust transition at fast-spreading ridges. Contrib. Mineral. Petrol. 136, 111–130.
Dare, S.A.S., 2007. Chrome-spinel Geochemistry of the Northern Oman-United Arab Emirates Ophiolite (Unpublished Ph.D. thesis). Cardiff University, Wales.
Dare, S.A.S., Pearce, J.A., McDonald, I., Styles, M.T., 2009. Tectonic discrimination of peridotites using fO_2-Cr# and Ga-Ti-Fe^{III} systematics in chrome-spinel. Chem. Geol. 261 (3–4), 199–216.
Derbyshire, E.J., O'Driscoll, B., Lenaz, D., Gertisser, R., Kronz, A., 2013. Compositionally heterogeneous podiform chromitite in the Shetland Ophiolite Complex (Scotland): implications for chromitite petrogenesis and late-stage alteration in the upper mantle portion of a supra-subduction zone ophiolite. Lithos 162–163, 279–300.
Dick, H.J.B., Bullen, T., 1984. Chromian spinel as a petrogenetic indicator in abyssal and alpine-type peridotites and spatially associated lavas. Contrib. Mineral. Petrol. 86, 54–76.
Dijkstra, A.H., Drury, M.R., Vissers, R.L.M., 2001. Structural petrology of plagioclase-peridotites in the West Othris Mountains (Greece): melt impregnation in mantle lithosphere. J. Petrol. 42, 5–24.
Dijkstra, A.H., Barth, M.G., Drury, M.R., Mason, P.R.D., Vissers, R.L.M., 2003. Diffuse porous melt flow and melt-rock reaction in the mantle lithosphere at a slow-spreading ridge: a structural petrology and LA-ICP-MS study of the Othris Peridotite Massif (Greece). Geochem. Geophys. Geosyst. 4 (8). http://dx.doi.org/10.1029/2001GC000278.
Falloon, T.J., Danyushevsky, L.V., Crawford, A.J., Meffre, S., Woodhead, J.D., Bloomer, S.H., 2008. Boninites and adakites from the Northern termination of the Tonga Trench: implications for adakite petrogenesis. J. Petrol. 49, 1–19.
Feig, S.T., Koepke, J., Snow, J.E., 2006. Effect of water on tholeiitic basalt phase equilibria: an experimental study under oxidizing conditions. Contrib. Mineral. Petrol. 152, 611–638.
Ferrière, J., Bertrand, J., Simantov, J., De Wever, P., 1988. Comparison entre les formations volcano–detritiques (Mélanges) du malm des Hellenides internes (Othrys, Eubee): implications geodynamics. Bull. Geol. Soc. Greece 20, 223–235.
Fryer, P., Saboda, K.L., Johnson, L.E., Mackay, M.E., Moore, G.F., Stoffers, P., 1990. Conical seamount: SeaMARC II, Alvin submersible, and seismic reflection studies. In: Fryer, P., Pearce, J.A., Stokking, L.B. (Eds.), Proc ODP, Init Repts, 125. College Station, TX (Ocean Drilling Program), pp. 69–80.
Gahlan, H.A., Arai, S., 2007. Genesis of peculiarly zoned Co, Zn and Mn-rich chromian spinel in serpentinite of Bou-Azzer ophiolite, Anti-Atlas, Morocco. J. Mineral. Petrol. Sci. 102, 69–85.
Gervilla, F., Padrón-Navarta, J.A., Kerestedjian, T., Sergeeva, I., González-Jiménez, J.M., Fanlo, I., 2012. Formation of ferrian chromite in podiform chromitites from the Golyamo Kamenyane serpentinite, Eastern Rhodopes, SE Bulgaria: a two-stage process. Contrib. Mineral. Petrol. 164 (4), 643–657.
González-Jiménez, J.M., Proenza, J.A., Gervilla, F., Melgarejo, J.C., Blanco-Moreno, J.A., Ruiz-Sánchez, R., Griffin, W.L., 2011. High-Cr and high-Al chromitites from the Sagua de Tánamo district, Mayarí-Cristal Ophiolitic Massif (eastern Cuba): constraints on their origin from mineralogy and geochemistry of chromian spinel and platinum-group elements. Lithos 125, 101–121.
González-Jiménez, J.M., Griffin, W.L., Locmelis, M., O'Reilly, S.Y., Pearson, N.J., 2012. LA-ICP-MS analysis on spinel from chromitites of different tectonic settings: their contrasted minor- and trace-elements compositions (Abstracts) In: Annual VM Goldschmidt Conference, Montréal, Canada.
González-Jiménez, J.M., Griffin, W.L., Proenza, J.A., Gervilla, F., O'Reilly, S.Y., Akbulut, M., Pearson, N.J., Arai, S., 2014. Chromitites in ophiolites: how, where, when, why? Part II. The crystallization of chromitites. Lithos 189, 140–158.
González-Jiménez, J.M., Barra, F., Garrido, L.N.F., Reich, M., Satsukawa, T., Romero, R., Salazar, E., Colás, V., Orellana, F., Rabbia, O., Plissart, G., Morata, D., 2016. A secondary precious and base metal mineralization in chromitites linked to the development of a Paleozoic accretionary complex in Central Chile. Ore Geol. Rev. 78, 14–40.
Green, T.H., 1976. Experimental testing of "equilibrium" partial melting of peridotite under water-saturated, high pressure conditions. Can. Mineral. 14, 255–268.
Grieco, G., Merlini, A., 2012. Chromite alteration processes within Vourinos ophiolite. Int. J. Earth Sci. 101 (6), 1–11.
Grivas, E., Rassios, A., Konstantopoulou, G., Vacondios, I., Vrahatis, G., 1993. Drilling for "blind" podiform chrome orebodies at Voidolakkos in the Vourinos ophiolite complex, Greece. Econ. Geol. 88, 461–468.
Hickey, R.L., Frey, F.A., 1982. Geochemical characteristics of boninite series volcanics; implications for their source. Geochim. Cosmochim. Acta 46, 2099–2116.
Hilakos, P., 1980. The Geology, Exploration and Exploitation of Podiform Chromite Deposits with Special Reference to the Chromite Deposits of Greece (Dissertation). pp. 107.
Horn, I., Foley, S.F., Jackson, S.E., Jenner, G.A., 1994. Experimentally determined partitioning of high field strength and selected transition elements between spinel and

basaltic melt. Chem. Geol. 117, 193–218.
Hynes, A.J., 1972. The Geology of Part of the Western Othris Mountains, Greece. Unpublished Ph.D. thesis. University of Cambridge, UK.
Ishikawa, T., Nagaishi, K., Umino, S., 2002. Boninitic volcanism in the Oman ophiolite: implications for thermal condition during transition from spreading ridge to arc. Geology 30, 899–902.
Ishizuka, O., Tani, K., Reagan, M.K., Kanayama, K., Umino, S., Harigane, Y., Sakamoto, I., Miyajima, Y., Yuasa, M., Dunkley, D.J., 2011. The timescales of subduction initiation and subsequent evolution of an oceanic island arc. Earth Planet. Sci. Lett. 306, 229–240.
Johan, Z., Dunlop, H., Le Bel, L., Robert, J.L., Volfinger, M., 1983. Origin of chromite deposits in ophiolitic complexes: evidence for a volatile- and sodium-rich reducing fluid phase. Fortschr. Mineral. 61, 105–107.
Kamenetsky, V.S., Crawford, A.J., Meffre, S., 2001. Factors controlling chemistry of magmatic spinel: an empirical study of associated olivine, Cr-spinel and melt inclusions from primitive rocks. J. Petrol. 42, 655–671.
Kapsiotis, A., Ewing-Rassios, A., Antonelou, A., Tzamos, E., 2016. Genesis and multi-episodic alteration of Zircon-bearing Chromitites from the Ayios Stefanos Mine, Othris Massif, Greece: assessment of an unconventional hypothesis on the origin of zircon in Ophiolitic Chromitites. Fortschr. Mineral. 6 (4), 124. http://dx.doi.org/10.3390/min6040124.
Kapsiotis, A., Ewing-Rassios, A., Grieco, G., Antonelou, A., 2017. Genesis of Cr-bearing hydrogrossular-rich veins in a chromitite boulder from Ayios Stefanos, West Othris, Greece: A Paradigm of Micro-rodingites Formation at the Late Stages of Oceanic Slab Emplacement. Ore Geol. Rev. http://dx.doi.org/10.1016/j.oregeorev.2017.06.006.
Koutsovitis, P., Magganas, A., 2016. Boninitic and tholeiitic basaltic lavas and dikes from dispersed Jurassic east Othris ophiolitic units, Greece: petrogenesis and geodynamic implications. Int. Geol. Rev. 58 (16), 1983–2006.
Leblanc, M., 1995. Chromite and ultramafic rock compositional zoning through a paleotransform fault, Poum, New Caledonia. Econ. Geol. 90, 2028–2039.
Leblanc, M., Nicolas, A., 1992. Ophiolitic chromites. Int. Geol. Rev. 34, 653–686.
Malpas, J., Robinson, P.T., Zhou, M.F., 1997. Chromite and ultramafic rock compositional zoning through a paleotransform fault, Poum, New Caledonia: discussion. Econ. Geol. 92, 502–503.
Malvin, D.J., Drake, M.J., 1987. Experimental determination of crystal/melt partitioning of Ga and Ge in the system forsterite-anorthite-diopside. Geochim. Cosmochim. Acta 51, 2117–2128.
Matveev, S., Ballhaus, C., 2002. Role of water in the origin of podiform chromitite deposits. Earth Planet. Sci. Lett. 203, 235–243.
Maurel, C., Maurel, P., 1982. Étude expérimentale de la distribution de l'aluminium entre bain silicaté basique et spinelle chromifère. Implications pétrogénétiques: teneur en chrome des spinelles. Bull. Mineral. 105, 197–202.
Mellini, M., Rumori, C., Viti, C., 2005. Hydrothermally reset magmatic spinels in retrograde serpentinites: formation of “ferritchromit” rims and chlorite aureoles. Contrib. Mineral. Petrol. 149, 266–275.
Menzies, M., 1973. Mineralogy and partial melt textures within an ultramafic-mafic body, Greece. Contrib. Mineral. Petrol. 42 (4), 273–285.
Menzies, M., Allen, C., 1974. Plagioclase lherzolite-residual mantle relationships within two eastern Mediterranean ophiolites. Contrib. Mineral. Petrol. 45, 197–213.
Moat, T., 1986. Appendix IX. Microfabric and Rock Deformation Studies: competency contrast and its control on structural behavior of mixed lithological sequences. In: Rassios, A., Roberts, S., Vacondios, I. (Eds.), The Application of a Multidisciplinary Concept for Chromite Exploration in the Vourinos Complex (N. Greece). Institute of Geology and Mineral Exploration, Athens, pp. 284–290.
Moores, E.M., 1969. Petrology and structure of the Vourinos ophiolite complex of Northern Greece. Geol. Soc. Am. Spec. Pap. 118, 1–74.
Mukherjee, R., Mondal, S.K., Rosing, M.T., Frei, R., 2010. Compositional variations in the Mesoarchean chromites of the Nuggihalli schist belt, Western Dharwar Craton (India): potential parental melts and implications for tectonic setting. Contrib. Mineral. Petrol. 160, 865–885.
Mukherjee, R., Mondal, S.K., González-Jiménez, J.M., Griffin, W.L., Pearson, N.J., O'Reilly, S.Y., 2015. Trace-element fingerprints of chromite, magnetite and sulfides from the 3.1 Ga ultramafic–mafic rocks of the Nuggihalli greenstone belt, Western Dharwar craton (India). Contrib. Mineral. Petrol. 169, 59. http://dx.doi.org/10.1007/s00410-015-1148-1.
Mysen, B.O., Kushiro, I., 1977. Compositional variations of coexisting phases with degrees of melting of peridotite in the upper mantle. Am. Mineral. 62, 843–865.
Niida, K., Green, D.H., 1999. Stability and chemical composition of pargasitic amphibole in MORB pyrolite under upper mantle conditions. Contrib. Mineral. Petrol. 135, 18–40.
Pagé, P., Barnes, S.J., 2009. Using trace-elements in chromites to constrain the origin of podiform chromitites in the Thetford Mines Ophiolite, Québec, Canada. Econ. Geol. 104, 997–1018.
Pearce, J., Barker, P.F., Edwards, S.J., Parkinson, I.J., Leat, P.T., 2000. Geochemistry and tectonic significance of peridotites from the South Sandwich arc-basin system, South Atlantic. Contrib. Mineral. Petrol. 139, 36–53.
Photiades, A., Saccani, E., Tassinari, R., 2003. Petrogenesis and tectonic setting of volcanic rocks from the Subpelagonian ophiolitic mélange in the Agoriani area (Othrys, Greece). Ofioliti 28, 121–135.
Pouchou, J.L., Pichoir, F., 1985. "PAP" correction procedure for improved quantitative microanalysis. In: Armstrong, J.T. (Ed.), Microbeam Analysis. San Francisco Press, San Francisco, California, USA, pp. 104–106.
Psyhogiopoulos, G., 1985. A Study of the Exploitation of the Chromitite Bodies of Metalleion (Domokos). ADDMBN, pp. 155.
Qiu, T., Zhu, Y., 2017. Chromian spinels in highly altered ultramafic rocks from the Sartohay ophiolitic mélange, Xinjiang, NW China. J. Asian Earth Sci. http://dx.doi.org/10.1016/j.jseaes.2017.08.011.
Quick, J.E., 1981. The origin and significance of large, tabular dunite bodies in the Trinity Peridotite, Northern California. Contrib. Mineral. Petrol. 78, 413–422.
Rassios, A., et al., The origin and mechanism promoting the formation of ophiolitic nappes: paradigm examples from the Mesohellenic Ophiolites (Greece), in preparation.
Rassios, A., Konstantopoulou, G., 1993. Emplacement tectonism and the position of chrome ores in the Mega Isoma peridotites, SW Othris, Greece. Bull. Geol. Soc. Greece 28, 463–474.
Rassios, A., Konstantopoulou, G., Vacondios, I., 1991. Tectonic Controls on Chrome Ore Localization in Ophiolites, Greece. Institute of Mining and Mineral Exploration, Athens, Greece, pp. 228.
Rassios, A., Charalampidis, P., Gerouki, F., Zabara, S., Gkika, I., 2003. Chrome Mines of Othris (Unpublished report for the E.U. Funded Study). IGME, Kozani, Greece, pp. 93.
Reagan, M.K., Ishizuka, O., Stern, R.J., Kelley, K.A., Ohara, Y., Blichert-Toft, J., Bloomer, S.H., Cash, J., Fryer, P., Hanan, B.B., Hickey-Vargas, R., Ishii, T., Kimura, J.I., Peate, D.W., Rowe, M., Woods, M., 2010. Fore-arc basalts and subduction initiation in the Izu-Bonin-Mariana system. Geochem. Geophys. Geosyst. 11, 1–17.
Reches, Z., Lockner, D.A., 2010. Fault weakening and earthquake instability by powder lubrication. Nature 467 (7314), 452–455.
Righter, K., Leeman, W.P., Hervig, R.L., 2006. Partitioning of Ni, Co and V between spinel-structured oxides and silicate melts: importance of spinel composition. Chem. Geol. 227, 1–25.
Rollinson, P., 2008. The geochemistry of mantle chromitites from the northern part of the Oman ophiolite: inferred parental melt compositions. Contrib. Mineral. Petrol. 156, 273–288.
Rollinson, H., Adetunji, J., 2015. The geochemistry and oxidation state of podiform chromitites from the mantle section of the Oman ophiolite: a review. Gondwana Res. 27, 543–554.
Rollinson, H., Appel, P.W.U., Frei, R., 2002. A metamorphosed, early archean chromitite from West Greenland: implications for the genesis of archean anorthositic chromitites. J. Petrol. 43, 1–28.
Saccani, E., 2015. A new method of discriminating different types of post-Archean ophiolitic basalts and their tectonic significance using Th-Nb and Ce-Dy-Yb systematics. Geosci. Front. 6, 481–501.
Saccani, E., Beccaluva, L., Photiades, A., Zeda, O., 2011. Petrogenesis and tectono-magmatic significance of basalts and mantle peridotites from the Albanian-Greek ophiolites and sub-ophiolitic mélanges. New constraints for the Triassic-Jurassic evolution of the Neo-Tethys in the Dinaride sector. Lithos 124, 227–242.
Schwab, B.E., Johnston, A.D., 2001. Melting systematics of modally variable, compositionally intermediate peridotites and the effects of mineral fertility. J. Petrol. 42, 1789–1811.
Shervais, J.W., 1982. Ti-V plots and the petrogenesis of modern and ophiolitic lavas. Earth Planet. Sci. Lett. 59, 101–118.
Singh, A.K., Singh, R.B., 2013. Genetic implications of Zn-and Mn-rich Cr-spinels in serpentinites of the Tidding Suture Zone, eastern Himalaya, NE India. Geol. J. 48 (1), 22–38.
Smith, A., 1979. Othris, Pindos and Vourinos ophiolites and the Pelagonian zone. In: 6th Colloquium on the Geology of the Aegean Region. Institute of Geological and Mining Research, Athens, Greece, pp. 1369–1374.
Smith, A.G., Rassios, A., 2003. The evolution of ideas for the origin and emplacement of the western Hellenic ophiolites. Geol. Soc. Am. Spec. Pap. 373, 337–350.
Smith, A.G., Hynes, A.J., Menzies, M., Nisbet, E.G., Price, I., Welland, M.J., Ferrière, J., 1975. The stratigraphy of the Othris Mountains, eastern central Greece: a deformed Mesozoic continental margin sequence. Eclogae Geol. Helv. 68, 463–481.
Spray, J.G., Bébien, J., Rex, D.C., Roddick, J.C., 1984. Age constraints on the igneous and metamorphic evolution of the Hellenic-Dinaric ophiolites. In: Dixon, J.E., Robertson, A.H.F. (Eds.), The Geological Evolution of the Eastern Mediterranean. Geol. Soc. Lon. S. Publ., vol. 17. pp. 619–627.
Stern, R.J., Reagan, M., Ishizuka, O., Ohara, Y., Whattam, S., 2012. To understand subduction initiation, study forearc crust: to understand forearc crust, study ophiolites. Lithosphere 4, 469–483.
Stowe, C.W., 1994. Compositions and tectonic settings of chromite deposits through time. Econ. Geol. 89, 528–546.
Ulmer, P., Trommsdorff, V., 1995. Serpentine stability to mantle depths and subduction-related magmatism. Science 268, 858–861.
Vergely, P., 1976. Origine «vardarienne», chevauchement vers l'Ouest et rétrocharriage vers l'Est des ophiolites de Macédoine (Grèce) au cours du Jurassique supérieur-Eocrétacé. C. R. Acad. Sci. Paris 280, 1063–1066.
Wasylenki, L.E., Baker, M.B., Kent, A.J.R., Stolper, E.M., 2003. Near solidus melting of the shallow upper mantle: partial melting experiments on depleted peridotite. J. Petrol. 44, 1163–1191.
Wendlandt, R.F., Eggler, D.H., 1980. The origin of potassic magmas: 2. Stability of phlogopite in natural spinel lherzolite and in the system $KAlSiO_4$-MgO-SiO_2-H_2O-CO_2 at high pressures and high temperatures. Am. J. Sci. 280, 421–458.
Whitney, D.L., Evans, B.W., 2010. Abbreviations for names of rock-forming minerals. Am. Mineral. 95, 185–187.
Xiong, Q., Henry, H., Griffin, W.L., Zheng, J.-P., Satsukawa, T., Pearson, N.J., O'Reilly, S.Y., 2017. High- and low-Cr chromitite and dunite in a Tibetan ophiolite: evolution from mature subduction system to incipient forearc in the Neo-Tethyan Ocean. Contrib. Mineral. Petrol. 172, 45. http://dx.doi.org/10.1007/s00410-017-1364-y.
Zaccarini, F., Garuti, G., Proenza, J.A., Campos, L., Thalhammer, O.A.R., Aiglsperger, T., Lewis, J., 2011. Chromite and platinum-group-elements mineralization in the Santa Elena ophiolitic ultramafic nappe (Costa Rica): geodynamic implications. Geol. Acta 9, 407–423.

Zhang, P.-F., Uysal, I., Zhou, M.-F., Su, B.-X., Avci, E., 2016. Subduction initiation for the formation of high-Cr chromitites in the Kop ophiolite, NE Turkey. Lithos 260, 345–355.
Zhou, M.F., Robinson, P.T., Bai, W.J., 1994. Formation of podiform chromitites by melt/rock interaction in the upper mantle. Mineral. Deposita 29, 98–101.
Zhou, M.F., Robinson, P.T., Malpas, J., Li, Z., 1996. Podiform chromitites from the Luobusa ophiolite (southern Tibet): implications for melt/rock interaction and chromite segregation in the upper mantle. J. Petrol. 37, 3–21.
Zhou, M.F., Robinson, P.T., Su, B.X., Gao, J.F., Li, J.W., Yang, J.S., Malpas, J., 2014. Compositions of chromite, associated minerals, and parental magmas of podiform chromite deposits: the role of slab contamination of asthenospheric melts in supra-subduction zone environments. Gondwana Res. 26 (1), 262–283.